博士論文

Doctoral Dissertation

Multi-Satellite Remote Sensing Techniques For Grassland Biomass Monitoring in Mongolia

マルチ衛星リモートセンシング技術による モンゴルの草原バイオマス監視

September, 2025

Margad-Erdene Jargalsaikhan

山口大学大学院創成科学研究科

The Graduate School of Sciences and Technology for Innovation,

Yamaguchi University

Acknowledgment

I express my deepest gratitude to my research supervisors, Prof. Masahiko Nagai and Prof. Dorj Ichikawa, for their unwavering guidance, patience, and encouragement throughout my three-year journey at Yamaguchi University. Their expertise and support were instrumental in navigating the challenges of this research.

I am profoundly thankful to my family for their constant love, encouragement, and sacrifices, which made this dissertation possible. Their support has been my foundation during my academic and research endeavors.

I extend my appreciation to my laboratory colleagues and peers at Yamaguchi University for their collaboration, insightful discussions, and camaraderie, which greatly enriched my research experience. Special thanks go to the field teams, the National University of Mongolia, and the Botanical Garden and Research Institute - Mongolian Academy of Sciences for their invaluable contributions to data collection and project execution.

Finally, I am deeply thankful to the Higher Engineering Education Development Project (M-JEED program) for granting me the opportunity to pursue this research and study in Japan, making this milestone possible.

Margad-Erdene Jargalsaikhan

30 April 2025

Abstract

Grasslands, vital for Mongolia's ecological and socioeconomic sustainability, face increasing degradation, necessitating advanced, accurate, and frequent monitoring solutions. Single-satellite data struggle with balancing spatial resolution and data demands for large-scale monitoring, despite daily imagery. High-resolution PlanetScope imagery (3.125 m) offers detailed spatial data but poses data management challenges, while low-resolution JPSS-VIIRS imagery (375 m) provides less storage-intensive daily data but lacks precision for biomass estimation, complicating validation with small ground plots. To address these limitations, this dissertation develops a novel multi-satellite approach by adapting a high-resolution PlanetScope biomass model to VIIRS imagery through spectral harmonization, monitoring aboveground biomass across Mongolia's grasslands. This integration optimizes spectral, spatial, and temporal coverage. A PlanetScope-based linear regression model, using NDVI and ground data from 85 plots, achieved R^2 values of 0.65, 0.82, and 0.80 for desert, dry, and mountain grasslands, respectively (combined R^2=0.62, RMSE=35.28 g/m²). Time-series analysis (2020–2024) revealed desert biomass declines from 62 g/m² to 33 g/m² and grazed-ungrazed gaps in desert regions (trend slope=0.12), indicating severe overgrazing-driven degradation. The innovative model adaptation to VIIRS, using optimized Spectral Band Adjustment Factors, aligned red band ranges (VIIRS: 600–680 nm; PlanetScope: 650–680 nm), reducing discrepancies from 6.2% to 4.8%. Harmonized VIIRS data estimated a five-year mean biomass of 71.4 g/m² across Mongolia, with Bag-level comparisons showing 10.5% higher estimates in the desert, 9.6% higher in dry, and 1.9% lower in mountain grasslands versus PlanetScope, with strong agreement (RMSE=11.6 g/m², mean difference=10.74%, R^2=0.92). This approach, with lower RMSE but limited variability in mountains and higher uncertainty in heterogeneous desert and dry regions, demonstrates the effectiveness and accuracy of the proposed methodology in bridging spatial and temporal gaps, providing a valuable tool for large-scale weekly grassland biomass monitoring with applicability beyond the Mongolian context.

Abbreviations

ADB ..... Aboveground Dry Biomass

BOA ..... Bottom of Atmosphere

BGRI-MAS ..... Botanic Garden and Research Institute – Mongolian Academy of Science

EO-1 ..... Earth Observation 1

GCP ..... Ground Control Point

GDP ..... Gross Domestic Product

HLS ..... Harmonized Landsat Sentinel-2

JPSS ..... Joint Polar Satellite System

MODIS ..... Moderate Resolution Imaging Spectroradiometer

NDVI ..... Normalized Difference Vegetation Index

NIR ..... Near Infrared

RMSE ..... Root Mean Square Error

RSR ..... Relative Spectral Response

SBAF ..... Spectral Band Adjustment Factor

SDR ..... Sensor Data Record

SR ..... Surface Reflectance

TOA ..... Top of Atmosphere

VIIRS ..... Visible Infrared Imaging Radiometer Suite

Contents

List of Figures

List of Tables

Chapter I. INTRODUCTION

1.1 Ecological Significance and Socioeconomic Role of Mongolian Grasslands in a Changing Global Context

Grasslands, spanning approximately 38% of Earth's land surface (52 million km², excluding Greenland and Antarctica), are vital terrestrial ecosystems encompassing prairies, savannas, and steppes [1]. They store substantial carbon in deep root systems and soils, contributing to the global carbon cycle and climate change mitigation, while stabilizing watersheds, preventing soil erosion, and supporting hydrological cycles [2, 3, 4]. These ecosystems balance ecological functions with human needs, yet face escalating threats from climate change, overgrazing, and land-use changes, necessitating advanced monitoring to ensure sustainability [5, 6, 7].

Mongolia, a landlocked Central Asian nation bordered by Russia and China, exemplifies this significance with its 112 million hectares of grasslands, covering 71.8% of its 1,562,950 km² land area [7, 8]. As part of the Eurasian steppe, the world's largest continuous grassland system, Mongolia's temperate grasslands support native species such as Stipa krylovii and Caragana microphylla, alongside fauna like the Siberian marmot (Marmota sibirica) and the endangered Mongolian gazelle (Procapra gutturosa) [1, 9]. Their ecological roles, including carbon sequestration and water regulation, are shaped by a continental climate with extreme temperature swings (- 4.3 to 5.3°C) and low precipitation (120 to 370 mm annually), creating resilient yet vulnerable ecosystems [10]. These grasslands align with global patterns, where semi-arid ecosystems are critical for biodiversity and ecosystem services but are increasingly at risk [11]. For instance, grasslands in the African Sahel and Australian outback face similar degradation pressures, highlighting the need for scalable monitoring solutions [12].

Socioeconomically, Mongolia's grasslands sustain a pastoral economy rooted in millennia of nomadic tradition, supporting 71 million livestock (sheep, goats, cattle, horses, camels) and driving food security through meat and dairy production [8]. Exports of wool and cashmere contribute significantly to GDP, with livestock-related activities accounting for approximately 30% of economic output [13]. The cultural heritage and scenic beauty of these grasslands fuel a growing ecotourism industry, attracting visitors to sites like Khustain Nuruu National Park and the Gobi Desert, diversifying income for rural communities [7]. These economic roles parallel global grassland-dependent societies, such as the Maasai in the

Serengeti or ranchers in Yellowstone, where pastoralism and tourism are economic pillars [14]. However, overgrazing and infrastructure development threaten these livelihoods, reducing biomass and forage availability, as evidenced by declining desert grassland productivity [7].

Climate shifts, including rising temperatures and altered precipitation patterns, threaten grassland productivity worldwide, with Mongolia's semi-arid ecosystems facing heightened risks due to their fragility [15]. Human pressures, such as overgrazing and infrastructure expansion (e.g., mining, roads), further test resilience, necessitating advanced monitoring tools [7]. Traditional ground-based methods in Mongolia, reliant on sparse measurements, lack the scale and frequency to address these pressures, while economic and technological limitations hinder integrated solutions [12, 15, 16]. This research leverages multi-satellite remote sensing techniques, integrating high-resolution PlanetScope (3.125 m) and low-resolution VIIRS (375 m) imagery through spectral harmonization, to quantify grassland biomass and support sustainable management, building on prior studies [7, 17]. Historically, Mongolia's grasslands have shaped its nomadic identity for over 3,000 years, with archaeological evidence highlighting their role as a cultural and ecological foundation, underscoring the need for innovative monitoring to preserve this legacy [18].

1.2 The current status of Mongolian Grasslands

Mongolia's grasslands, spanning 112 million hectares (71.8% of its land area), are vital to its ecological and cultural identity [8]. These temperate ecosystems are divided into five types: high mountain, mountain, dry steppe, meadow, and desert. This study focuses on three main types: desert (25.41%, Gobi region, 120 to 200 mm precipitation, 0.6 to 5.3°C, Gobi brown soils, sparse Caragana microphylla), dry steppe (22.05%, central Mongolia, 200 to 270 mm, minus 2.6 to 1.2°C, chestnut soils, Stipa krylovii), and mountain grasslands (12.99%, Khentii Mountains, 130 to 370 mm, minus 4.3 to minus 3.6°C, dark chestnut soils, dense vegetation) [9]. These grasslands sustain Mongolia's pastoral economy and biodiversity but are under significant degradation pressures [7].

National assessments report that approximately 60% of grasslands are degraded, with 75% of grasslands affected by desertification, driven by overgrazing, climate change, and infrastructure [15, 16]. Overgrazing, with livestock numbers exceeding sustainable levels (71 million head), strips vegetation, particularly in desert regions where sparse cover offers little

resilience, while mountain grasslands resist better due to higher moisture [7]. Time-series analysis (2020 to 2023) revealed desert biomass declines from 62 g/m^2 to 33 g/m^2, with widening grazed-ungrazed biomass gaps (slope 0.12), indicating severe degradation [7]. Climate change intensifies these impacts, with reduced precipitation, rising temperatures, and frequent extreme events (droughts, dzuds) diminishing productivity over two decades [15]. The COP21 projection of a 2°C global temperature rise threatens further disruptions, exacerbating desertification [19].

Infrastructure projects, such as the Oyu Tolgoi copper-gold mine in the Gobi, alongside road construction and urban expansion, fragment habitats and accelerate soil erosion [20]. The mine diverts water and generates dust pollution, impacting local ecosystems and species like the Mongolian gazelle, which face reduced forage and shrinking ranges [7]. These pressures underscore the need for comprehensive, scalable monitoring data to inform management strategies [17]. Comparative studies in other semi-arid regions, such as Kazakhstan's steppes, show similar mining-related degradation, highlighting the global relevance of Mongolia's challenges [21].

Current monitoring at the BGRI-MAS sites in Olon-Ovoo Bag (desert), Lkhumbe Bag (dry), and Jargalant Bag (mountain) relies on ground-based methods, where biomass is collected using the hand-harvesting method in specific field areas, including both ungrazed and grazed plots [7]. Since 2009, BGRI-MAS has annually gathered data on biomass, vegetation cover, and plant classification, collecting wet biomass and litter in the field, separating plants and litter, and drying wet plants in the laboratory to obtain dry biomass [7]. These surveys, constrained by remote terrain, harsh weather, and limited coverage, fail to capture rapid degradation dynamics across 112 million hectares [17]. Data fragmentation among institutions and economic-technological constraints further limit analysis [15]. Government initiatives, like the Green Belt Project (2005), show localized success in curbing desertification through reforestation and restoration but require scalable monitoring to evaluate impacts across diverse grasslands [15]. This research employs multi-satellite remote sensing, integrating PlanetScope and VIIRS, to deliver weekly, large-scale biomass assessments, addressing these gaps [17].

Additionally, the Mongolian government's Land Monitoring Unit, part of the Agency for Land Administration and Management, Geodesy, and Cartography, conducts nationwide ground-based monitoring to assess grassland condition, quality, and land use changes, in

alignment with legal frameworks [22]. This unit maintains a photo-monitoring database for pasturelands, develops unified assessments, and provides policy recommendations for land protection and rehabilitation, incorporating limited remote sensing and modern technologies to track ecological changes [22]. Activities include expanding monitoring networks, managing soil analysis laboratories, and collaborating with professional organizations to evaluate environmental impacts, such as those from grazing or infrastructure [22]. Despite these efforts, the unit's reliance on ground-based methods and challenges in data integration and national-scale coverage limit its ability to address rapid degradation dynamics, further highlighting the need for scalable, satellite-based solutions like those proposed in this study [17].

1.3 Quantitative Assessment of Grassland Condition

Effective monitoring of Mongolian grasslands requires a quantitative approach to address their vast scale, ecological diversity, and rapid degradation [16]. Qualitative observations, such as visual surveys and anecdotal reports, lack the precision and coverage needed to track changes across 112 million hectares or respond to environmental shifts, whereas quantitative assessment provides structured, measurable data to reveal trends, assess ecosystem health, and guide management with detail unattainable through descriptive methods [4, 15]. This is critical for Mongolia, where logistical challenges, including remote terrain and harsh climate, combined with limited resources, hinder traditional monitoring, underscoring the need for scalable, data-driven strategies [15]. Global studies, particularly in Inner Mongolia, highlight the efficacy of quantitative remote sensing for grassland management, reinforcing its necessity for capturing spatial and temporal dynamics in semi-arid regions [23].

Aboveground biomass, the primary metric of this study, quantifies living plant material, serving as a key indicator of productivity, carbon storage, and forage availability, directly relevant to Mongolia's ecological and socioeconomic priorities [3, 7]. Literature on biomass estimation underscores its role in assessing grassland health, with remote sensing enabling large-scale monitoring through platforms like MODIS, Sentinel-2, Landsat, and high-resolution PlanetScope imagery [7, 24]. Parametric models, such as linear regression, correlate satellite-derived indices like NDVI with field-measured biomass, offering simplicity but sensitivity to grazing variability and small-scale ground data mismatches, particularly in Mongolia's heterogeneous grasslands [7]. Non-parametric models, including random forest and artificial neural networks, integrate multiple parameters for improved accuracy but require extensive

computational resources and training data, posing challenges for resource-constrained regions [7]. Studies in Mongolia highlight difficulties with coarse-resolution sensors (e.g., MODIS 250 m), which struggle to capture fine-scale variations, while high-resolution data (e.g., PlanetScope 3.125 m) better align with 1 m^2 field plots, though storage and processing demands limit scalability [7, 24]. These findings emphasize the need for tailored approaches to address Mongolia's unique ecological and logistical constraints, informing this study's focus on multi-satellite integration.

Further literature reveals the evolution of biomass estimation techniques tailored to Mongolia's semi-arid grasslands, where spatial heterogeneity and grazing pressures complicate monitoring efforts [7, 24]. High-resolution platforms like PlanetScope enable precise mapping of small-scale variations, critical for detecting degradation in sparse desert regions, but face challenges in data management and cost, prompting exploration of multi-sensor integration with platforms like VIIRS for broader coverage [7]. Advanced methods, such as partial least squares regression and machine learning, have been applied to integrate vegetation indices (e.g., Enhanced Vegetation Index, Green Chlorophyll Index) with environmental variables, improving model robustness but requiring extensive ground validation, which is logistically challenging in remote areas [7]. Research in Inner Mongolia using MODIS highlights the trade-off between temporal frequency and spatial detail, underscoring the potential of hybrid approaches that combine high- and low-resolution data to balance accuracy and scalability, a strategy this study advances through spectral harmonization [24]. These insights guide the development of monitoring frameworks suited to Mongolia's pastoral landscapes, addressing gaps in traditional methods.

Vegetation cover measures soil protection, influencing erosion resistance and habitat quality, while species composition reflects biodiversity and resilience, and parameters like leaf area index (LAI) and net primary productivity (NPP) capture canopy density and plant growth rates, respectively [4, 5]. These parameters, quantifiable via remote sensing, provide a comprehensive view of grassland condition amidst environmental pressures, with indices like NDVI serving as proxies for biomass and productivity due to their sensitivity to plant vigor in semi-arid regions [6, 25, 26]. Biomass is prioritized for its ability to capture combined effects of overgrazing, climate, and infrastructure, offering a practical measure for grazing management and restoration, as demonstrated by studies in the Tibetan Plateau [7, 27]. This

study leverages satellite-based biomass quantification to provide a scalable foundation for sustainable grassland management, addressing Mongolia's pressing degradation challenges.

1.4 Multi-Satellite Remote Sensing Technology for Grassland Monitoring

Satellite remote sensing surpasses ground-based methods by assessing vegetation health, land cover, and ecological parameters over vast regions with consistent observations, offering extensive spatial coverage critical for Mongolia's 112 million hectares of grasslands and flexible temporal resolution that enables dynamic change tracking and near-real-time monitoring [1, 4]. This approach reduces fieldwork logistics, provides cost-effective large-scale solutions, and delivers timely data when processed efficiently, making it indispensable for monitoring expansive and dynamic ecosystems [5]. However, single-satellite systems encounter significant challenges, including resolution trade-offs between spatial detail and coverage, as well as cloud cover in variable climates, which limit their effectiveness for comprehensive grassland monitoring [6]. For instance, low-resolution satellites like VIIRS, with a 375 m resolution and daily revisits, provide frequent, broad coverage but struggle to capture fine-scale variability in sparse desert grasslands, complicating validation against small 1 m^2 ground plots [7, 17]. Conversely, high-resolution satellites like PlanetScope, offering 3.125 m resolution and daily imagery, deliver detailed data capable of detecting subtle vegetation changes, but their limited swath width, high storage requirements, and associated costs hinder application over regional scales [7, 17]. Ground truth data, essential for calibration, are typically collected at small scales, creating mismatches with both high- and low-resolution systems and necessitating innovative integration strategies [26]. Global applications, such as grassland monitoring in Australia's rangelands, demonstrate remote sensing's potential but underscore the necessity of multi-sensor approaches to overcome these limitations and achieve robust, scalable solutions [28].

Multi-satellite approaches address these challenges by combining the strengths of enhanced spatial-temporal coverage and data robustness, integrating VIIRS's daily, cloud-free data with PlanetScope's high-resolution snapshots to ensure timely and precise monitoring, as evidenced by successful adaptations of high-resolution models to low-resolution systems in studies combining Landsat and MODIS for grassland biomass estimation [4, 17, 29].

Integrating data from sensors with differing spectral characteristics, such as VIIRS (red: 600 to 680 nm; NIR: 845 to 885 nm) and PlanetScope (red: 650 to 680 nm; NIR: 845 to 885 nm), requires spectral harmonization to mitigate discrepancies in reflectance and vegetation indices arising from variations in RSR, which can otherwise compromise monitoring accuracy [17]. This study employs the SBAF method, designed specifically for grasslands, to align VIIRS and PlanetScope imagery, leveraging hyperspectral Hyperion data and sensor RSR profiles to simulate sensor-specific reflectance through weighted integration and Gaussian-modeled RSR, followed by SBAF calculations for red and NIR bands, as detailed in recent research and discussions on grassland-specific tuning [17, 30]. The method optimizes harmonization by classifying surfaces into grassy (NDVI $\geq$ 0.3), bare (0.12 < NDVI < 0.3), and sandy (NDVI $\leq$ 0.12) areas, tailoring adjustments to grassland spectral behavior, where red reflectance decreases in grassy areas and increases in bare areas, ensuring precise alignment for Mongolia's diverse ecosystems [17].

The selection of the SBAF method reflects its simplicity, interpretability, and effectiveness in grassland applications, as it employs a straightforward linear adjustment based on hyperspectral data, suitable for large-scale monitoring with limited computational resources, unlike more complex methods that demand extensive processing, as noted in discussions on optimization strategies [17, 26, 30]. By leveraging NDVI thresholds derived from Hyperion and field measurements, with grassy areas averaging NDVI $\approx$ 0.568 and bare areas $\approx$ 0.237, SBAF addresses the pronounced red-NIR reflectance sensitivity of Mongolia's grasslands, building on established cross-sensor calibration techniques that have proven effective in diverse remote sensing contexts [17, 30]. Alternative harmonization methods, such as simple linear regression used in the HLS product, adjust reflectance statistically but lack ecosystem-specific tuning, resulting in reduced accuracy in heterogeneous grasslands [17, 31]. The Spatial and Temporal Adaptive Reflectance Fusion Model (STARFM), which blends Landsat and MODIS data for daily 30 m imagery, excels in areas with gradual changes but struggles with rapid grassland dynamics, such as drought-induced vegetation shifts, and its computational complexity limits scalability compared to SBAF's streamlined approach, which supports efficient processing across large regions [17, 29]. Machine learning methods, including random forest and deep learning, model complex spectral relationships and show promise globally, yet require large training datasets and computational resources, with performance in grasslands less optimized compared to SBAF's tailored design, as highlighted in discussions on harmonization

challenges [17, 32]. The HLS dataset, harmonizing Landsat and Sentinel-2 at 30 m resolution, is constrained by 5–16 day revisit cycles, insufficient for weekly grassland monitoring, whereas SBAF's application to daily VIIRS data supports the frequent observations critical for Mongolia's dynamic ecosystems [17, 31].

The SBAF method enables the adaptation of high-resolution biomass models to low-resolution imagery, facilitating scalable monitoring across Mongolia's diverse grassland zones, with potential applications in other semi-arid regions like Kazakhstan's steppes, as supported by its ability to integrate detailed and frequent data [17, 21]. Despite its strengths, the method relies on Hyperion data, which may have gaps, and excludes off-nadir observations, potentially introducing variability, as noted in discussions on methodological limitations [17]. Future research could explore machine learning to enhance harmonization accuracy across heterogeneous landscapes, building on suggestions for integrating advanced algorithms to refine large-scale monitoring frameworks, thereby extending the applicability of this approach to diverse ecological contexts [17]. By harmonizing high- and low-resolution data, this research delivers scalable solutions that achieve both spatial detail and temporal frequency, addressing the critical need for sustainable grassland management in Mongolia and beyond [17].

1.5 Research Objective and Novelty

This dissertation aims to develop a comprehensive methodology for frequent, accurate, and large-scale grassland biomass monitoring in Mongolia by integrating the enhanced spatial-temporal coverage and data robustness of high-resolution PlanetScope and low-resolution VIIRS imagery through model adaptation with spectral harmonization [17]. Mongolia's grasslands, crucial for ecological balance and socioeconomic stability, as noted earlier, face increasing pressures from overgrazing, climate variability, and infrastructure expansion, demanding advanced monitoring beyond the scope of traditional methods [7]. Building on the quantitative assessment needs and multi-satellite potential outlined previously, this study addresses current monitoring gaps by merging the strengths of high- and low-resolution satellite systems. The methodology strives to provide scalable weekly monitoring with an accurate assessment, enhancing sustainable grassland management and offering potential applications for other semi-arid regions worldwide.

The specific objectives of this research are fourfold, each targeting a vital component of the monitoring process. First, the study focuses on developing a biomass estimation model using high-resolution PlanetScope imagery, which delivers detailed spatial data frequently, achieving strong correlations with ground measurements for desert, dry, and mountain grasslands [7]. This objective sets the foundation for capturing fine-scale biomass variations, essential for understanding grassland productivity and health locally, and demonstrates the power of high-resolution PlanetScope satellite imagery to reveal intricate ecological patterns. Second, spectral harmonization integrates high-resolution PlanetScope imagery with low-resolution VIIRS imagery, focusing on red and NIR bands in grasslands, to align their differing spectral radiometric characteristics. This process adapts a PlanetScope data-driven biomass model to VIIRS imagery, producing P375 SR (VIIRS SR harmonized to PlanetScope at 375 m resolution with daily observations) for frequent, accurate, and large-scale assessments [17]. This step enhances monitoring frequency and coverage by leveraging the complementary strengths: PlanetScope's high spatial resolution and VIIRS's daily broad coverage. Third, the research examines the impact of grazing on Mongolian grasslands, by assessing how livestock pressure affects biomass across diverse ecological zones and evaluating degradation through comparing grazed and ungrazed areas in various grassland types, identifying trends essential for land management [7]. Fourth, the study aims to develop near-real-time weekly time series mapping across Mongolia's entire grassland region, capturing temporal and spatial biomass changes to provide a dynamic perspective of grassland conditions and their responses to environmental and human influences over time [17]. Taken together, these objectives establish a weekly grassland biomass monitoring framework across Mongolia, effectively integrating high spatial resolution with consistent broad temporal coverage.

The novelty of this dissertation comes from its integration of multi-satellite data and its tailored application to grassland biomass monitoring. A key contribution is the unique use of classified spectral harmonization between high-resolution PlanetScope and low-resolution VIIRS imagery for grasslands, optimizing data alignment through NDVI-based grassland categorization [17]. While spectral harmonization has been applied elsewhere, this specific combination in grassland ecosystems is new, combining detailed local insights with frequent, large-scale observations [26]. Another new aspect is adapting a high-resolution PlanetScope biomass model to a low-resolution VIIRS framework [7]. This method overcomes the

drawbacks of single-satellite systems, where high-resolution models lack broad coverage and low-resolution data lack precision, delivering a practical and balanced solution.

Additionally, this research provides a satellite-based grassland monitoring framework that combines ecological diversity with practical benefits, enhancing its originality. It delivers a flexible toolset by tailoring the methodology to varied grassland types, such as sparse desert and dense mountain zones, and incorporating grazing impact comparisons and near-real-time time series mapping. This enables proactive management, including early warning systems for degradation, with potential applications in semi-arid regions like the Sahel and Kazakhstan [26]. Its focus on scalability, linking local accuracy to national coverage, offers a repeatable model for policymakers and researchers, advancing grassland management capabilities. This research thus contributes by integrating a multi-satellite strategy, adapting models with spectral radiometric harmonization, and providing an ecologically responsive solution for sustainable conservation.

Chapter II. METHODOLOGY

This chapter outlines the methodology developed to achieve the objectives of this dissertation: establishing a robust framework for frequent, accurate, and large-scale grassland biomass monitoring in Mongolia. The approach adapts a high-resolution PlanetScope biomass estimation model [7] to low-resolution VIIRS imagery through spectral harmonization [17]. The methodology integrates high-resolution PlanetScope satellite data with field-measured ground data for biomass estimation, followed by spectral harmonization using SBAF to adapt the model to VIIRS SR at 375 m resolution (P375). This approach enables weekly biomass monitoring and grassland mapping across Mongolia. The study also includes time-series analysis of grassland dynamics and optimization of spectral harmonization for Mongolian

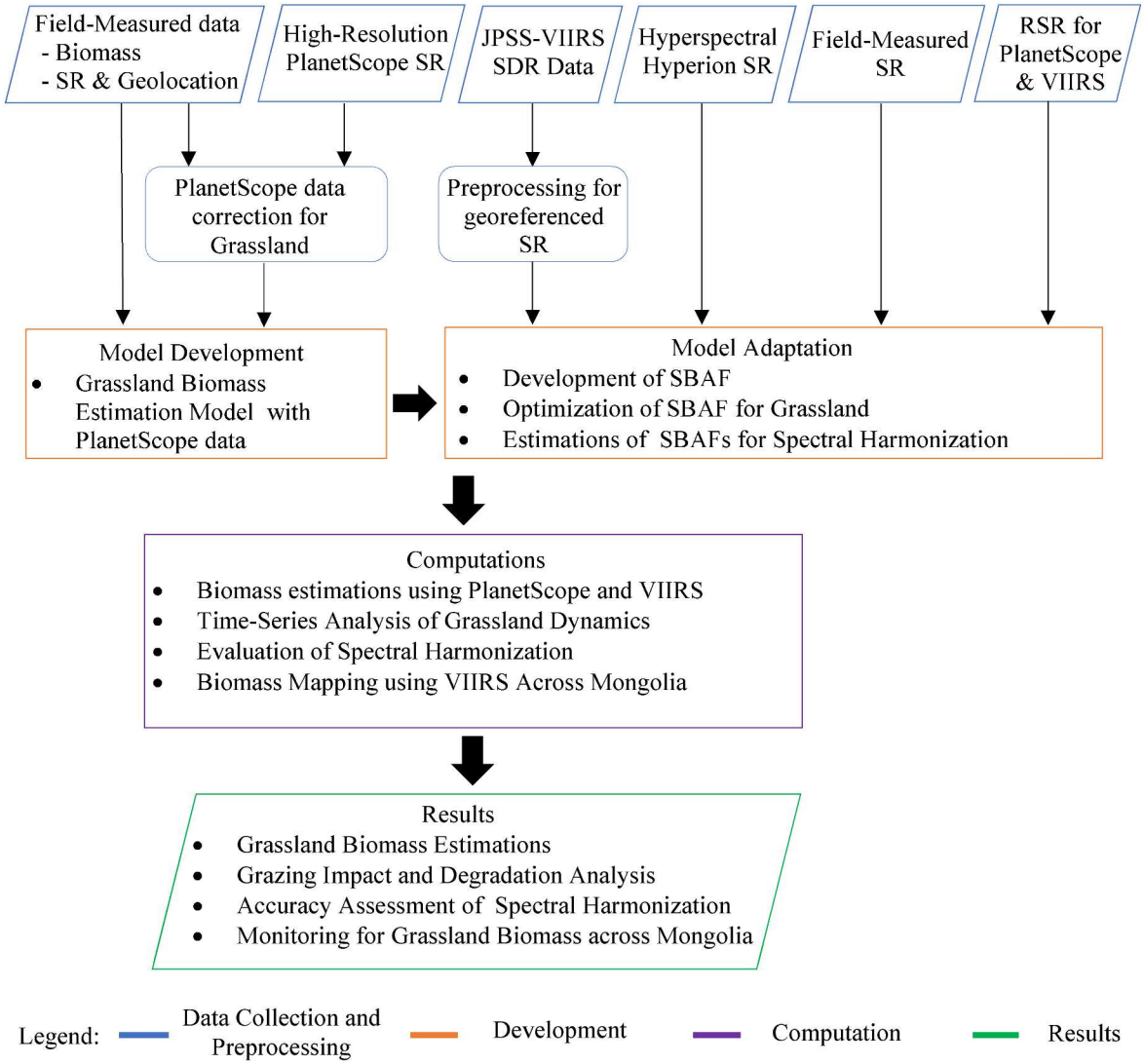

Figure 1. Flow diagram of Methodology

grasslands. The workflow is summarized in Figure 1, detailing the sequential steps of data collection, preprocessing, model development, computation, and results.

Data Collection and Preprocessing

Data collection: Building upon the multi-satellite framework introduced in Chapter 1, this study integrates diverse satellite datasets, including PlanetScope SuperDove, JPSS-VIIRS, and Hyperion EO-1, along with sensor-specific technical data such as RSR. These are combined with ground-based measurements of aboveground dry biomass, surface reflectance, and geolocation coordinates collected from Mongolia's grasslands [7, 17].

- Field-Measured Data: Includes aboveground biomass for model development, surface reflectance for radiometric correction, and geolocation coordinates for geometric correction.
- PlanetScope Data: Supports biomass estimation model development, spectral harmonization evaluation, and time-series analysis for grassland dynamics and mapping.
- JPSS-VIIRS Data: Used for large-scale biomass mapping, weekly monitoring, and spectral harmonization evaluation across Mongolia's grasslands.
- Hyperspectral Hyperion EO-1 Data: Combined with RSR profiles of VIIRS and PlanetScope to simulate spectral reflectance for SBAF estimation and optimization in grasslands.
- Field-measured SR Data: Collected by the research team and sourced from RedCalNet, used to estimate NDVI thresholds for SBAF optimization.
- RSR for PlanetScope & VIIRS: Technical data for SBAF estimation.

Preprocessing: Accurate biomass estimation requires corrected satellite data converted to surface reflectance. Preprocessing was applied to PlanetScope and VIIRS SDR Level 1B data.

- PlanetScope Data Correction: Cloud-free Ortho Tile and Scene images underwent geometric registration using GCPs (white square sheets). Radiometric correction of red and NIR bands used field-measured surface reflectance [7].
- JPSS-VIIRS SDR L1B Data Preprocessing: SDR data were transformed to georeferenced surface reflectance by converting TOA reflectance to BOA and georeferencing to an Earth-projected coordinate system [17].

Development

Biomass Estimation Model Development: A high-resolution biomass estimation model was developed using simple linear regression [34], correlating PlanetScope's NDVI with ground-measured biomass [7]. The model targets Mongolia's desert, dry steppe, and mountain grasslands. It leverages field data from 85 1×1 m plots at BGRI-MAS sites (2020–2023) and 343 PlanetScope images to ensure precision for VIIRS integration [7].

Model Adaptation: The PlanetScope biomass model was adapted to VIIRS imagery through spectral harmonization with SBAF [17].

- Development of SBAF: SBAFs were calculated using Hyperion data and RSR profiles of PlanetScope and VIIRS to account for spectral differences [17].
- Optimization of SBAF for Grassland: SBAFs were optimized by classifying surfaces into grassy and bare areas using NDVI thresholds, enhancing accuracy [17].
- Estimation of SBAF: Optimized SBAFs were applied to VIIRS reflectance to harmonize it with PlanetScope imagery, resulting harmonized VIIRS SR (P375) that enabling model adaptation [17].

Computation

This section outlines the analytical methods employed in the study. The following computations were performed:

Biomass estimations using PlanetScope and VIIRS: The biomass estimation model was applied to Mongolia's 'Bag' administrative units, covering mountain, dry, and desert grasslands. PlanetScope and harmonized VIIRS imagery were used for accurate biomass estimation and time-series mapping to analyze spatial variability [7, 17]. For VIIRS biomass estimation, PlanetScope-derived biomass served as reference data, enabling uncertainty analysis by comparing the two datasets [17].

Time-Series Analysis of Grassland Dynamics: This computation analyzed grassland dynamics by processing data from grazed and ungrazed (fenced) plots at BGRI-MAS sites across mountain, dry steppe, and desert grasslands. Using 343 PlanetScope images from the 2020–2023 growing seasons, high-resolution time-series data were generated to assess grazing

impacts and degradation trends [7]. The analysis supports sustainable grassland management strategies.

Evaluation of Spectral Harmonization: Optimized and non-optimized SBAF approaches were applied to harmonize VIIRS to PlanetScope imagery, with evaluations conducted for grassland regions from 2020 to 2023. The comparison of PlanetScope imagery and VIIRS imagery before and after harmonization determines whether optimized SBAFs improve harmonization results.

Grassland Biomass Mapping Utilizing VIIRS Across Mongolia: A maximum NDVI 7-day cloud-free mosaic approach was employed to produce clear imagery across Mongolia. Spectral harmonization was applied to adapt the VIIRS data for the PlanetScope biomass estimation model. This approach enables weekly monitoring of grassland biomass across Mongolia [17].

Results (Outputs)

Grassland Biomass Estimations: A biomass estimation model driven by PlanetScope was developed and applied to generate biomass maps across the 'Bag' area in three grassland types, utilizing PlanetScope and harmonized VIIRS imagery. Comparing the two datasets reveals differences and quantifies uncertainty in VIIRS biomass estimation [7, 17].

Grazing Impact and Degradation Analysis: Time-series graphical plots illustrated degradation patterns, comparing grazed and ungrazed areas across three grassland types. Trend lines highlighted the influence of grazing and human activities, identifying regions with higher degradation levels [7].

Accuracy Assessment of Spectral Harmonization: Quantitative results and plots compare red, NIR, and NDVI values, demonstrating that optimized SBAF harmonization outperforms non-optimized SBAF harmonization [17].

Monitoring for Grassland Biomass across Mongolia: Weekly biomass and NDVI mapping from 2020 to 2024, utilizing harmonized VIIRS data, covering Mongolia. The approach proved effective for large-scale, frequent biomass monitoring [17].

This methodology provides a scalable and accurate framework, supporting Mongolia's ecological sustainability and land management [17].

Chapter III. STUDY AREA

3.1 Monitoring area: Mongolian Grassland

Mongolia was selected as the study area to align with the objectives of monitoring grassland biomass. Located between 41°34′ to 52°09′ N latitude and 87°45′ to 119°56′ E longitude, it spans 1,562,950 km², with grasslands covering 112 million hectares [8, 9]. Figure 2 shows its geography. The population is 3,544,835, with 249,450 herder households managing 57.6 million livestock [7, 8]. Nomadic herding, a cultural and economic pillar, relies on livestock, making Mongolia a major grazing nation [7].

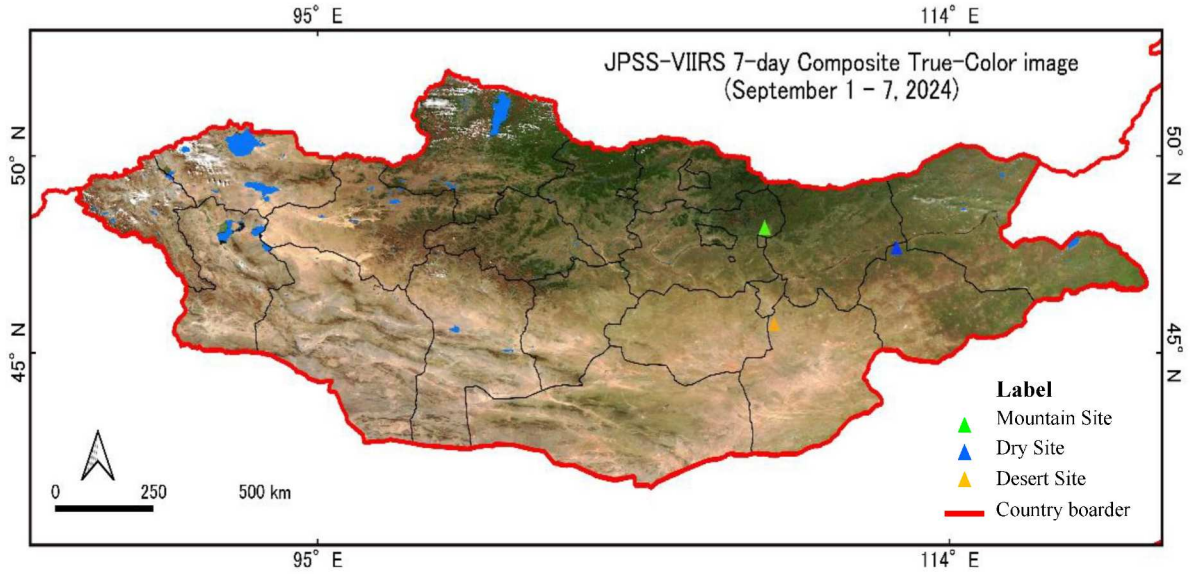

Figure 2. Study area, Mongolia

The climate includes subarctic, arid, and semi-arid zones with extreme variations [10]. Annual temperatures average -0.4°C to 2.8°C, with winters (December–February) dropping to -30°C to -40°C and summers (June–August) reaching 20°C to 40°C in the Gobi Desert [10]. Precipitation averages 150–450 mm, mostly in summer, with the Gobi Desert below 200 mm

(a) (b) (c)

Figure 3. Nomadic herding in Mongolian grasslands: (a) desert grassland, (b) dry steppe, (c) herding practice.

and northern mountains up to 450 mm [10, 15]. Low humidity (30–50%) and spring winds cause dust storms and dzud, impacting livestock [15]. Snow covers mountains for 4–5 months, but is minimal in the south [10].

Mongolia's grasslands, supporting biodiversity and carbon storage for nomadic herding, are shown in Figure 3. Nomadic herding in Mongolian grasslands: (a) desert grassland, (b) dry steppe, (c) herding practice. [7, 11]. Varied steppe ecosystems face degradation from overgrazing and climate variability [11, 15]. This study monitors these grasslands to guide sustainable management.

3.2 Experimental Sites for Model Development and Designated Analysis

The study focused on three grassland types: desert grassland (25.41% of Mongolia), dry steppe (22.05%), and mountain grassland (12.99%), collectively covering ~60% of Mongolia's land area and 83% of its grasslands [8, 9]. Field surveys were conducted at long-term vegetation monitoring sites managed by the Botanic Garden and Research Institute, Mongolian Academy of Sciences (BGRI-MAS), located in these grassland types, as shown in Figures 1, Figure 4 and 5.

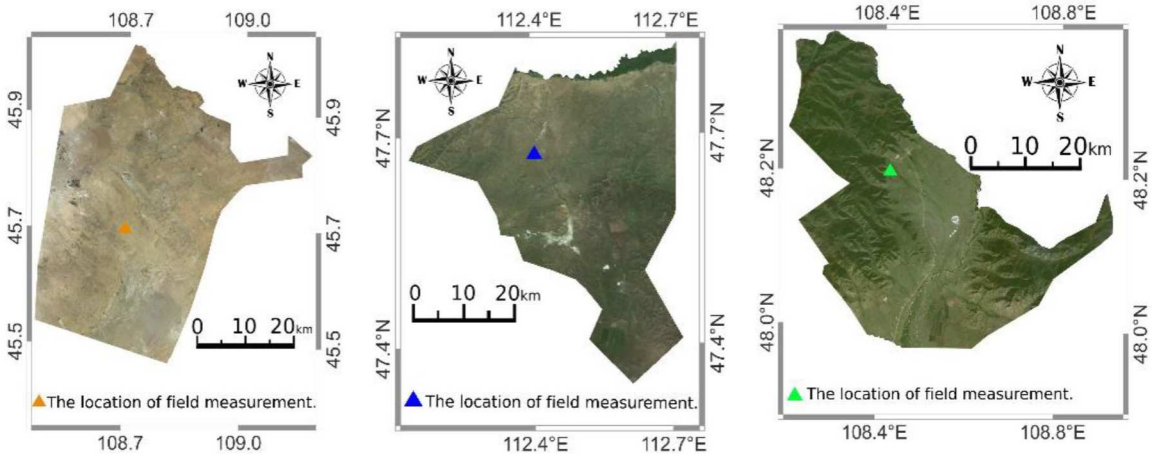

(a) Desert grassland **(b)** Dry grassland **(c)** Mountain grassland

Figure 4. BGRI-MAS field site locations (PlanetScope imagery): (a) Desert grassland, Olonovoo bag, Dalanjargalan Soum, 31 August 2023, (b) Dry grassland, Lkhumbe bag, Tumentsogt Soum, 1 September 2023, (c) Mountain grassland, Jargalant bag, Mungunmorit Soum, 1 September 2023.

BGRI-MAS, a leading institute for vegetation and soil research since 1970, maintains sites with ungrazed (fenced) and grazed areas [7]. Established in 2009 (dry steppe and mountain grassland, 1 ha) and 2010 (desert grassland, 0.5 ha), these sites support studies of grazing impacts [7]. Selected for ecological representativeness based on soil and vegetation data, the sites include:

- Desert Grassland: 120–200 mm annual precipitation, 0.6 to 5.3°C mean temperature, Gobi brown soil, low vegetation cover [10].
- Dry Grassland: 200–270 mm annual precipitation, -2.6 to 1.2°C mean temperature, chestnut soil, moderate vegetation cover [10].
- Mountain Grassland: 130–370 mm annual precipitation, -4.3 to -3.6°C mean temperature, dark chestnut soil, high vegetation cover [10].

At these sites, we collected biomass, surface reflectance, and geolocation data to develop and validate the biomass model [7]. BGRI-MAS has annually collected ground data, including vegetation biodiversity, cover, classification, and soil characteristics, since 2009 [7]. Figure 5 illustrates vegetation differences between grazed and ungrazed areas, with ungrazed plots showing denser cover, particularly in the desert grassland. These sites were chosen for

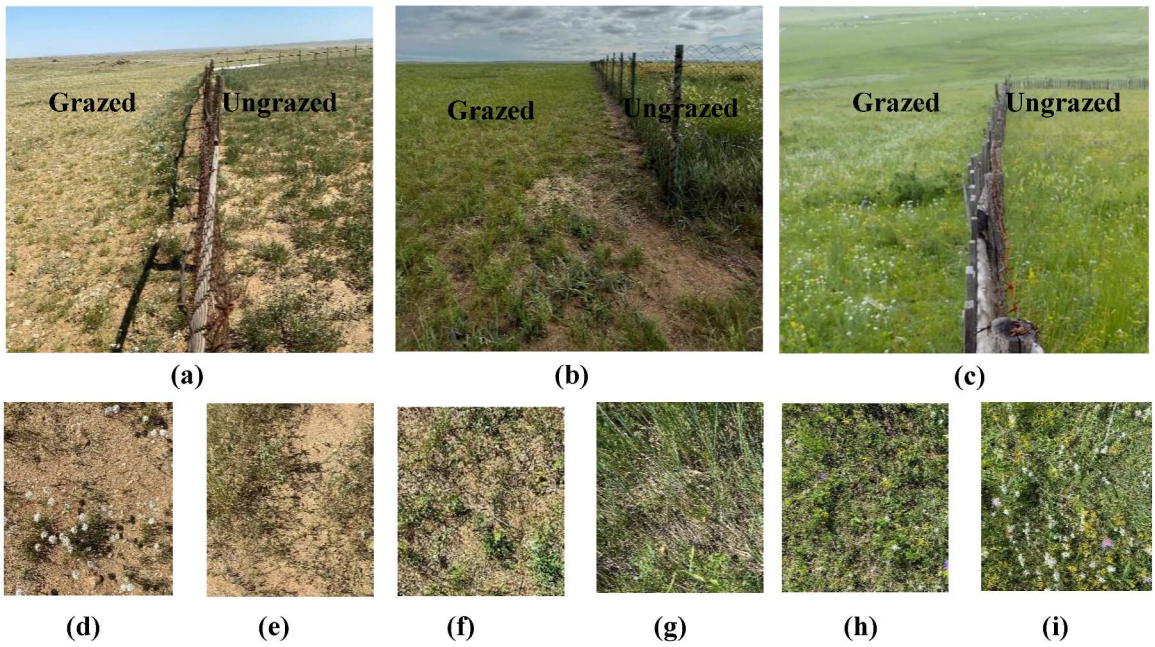

Figure 5. Top-down views of study site grasslands: (a) Desert grassland, (b) Dry grassland, (c) Mountain grassland, (d) Grazed desert grassland, (e) Ungrazed desert grassland, (f) Grazed dry grassland, (g) Ungrazed dry grassland, (h) Grazed mountain grassland, (i) Ungrazed mountain grassland.

their representativeness and robust fieldwork infrastructure, supporting the study's monitoring objectives [7, 17].

3.3 Calibration Sites for Spectral Harmonization

For spectral harmonization, field-measured surface reflectance data were utilized for optimization of SBAF [17]. Table 1 lists the coordinates of four field sites, and Figures 4 and 6 show their geographic distribution. Three sites, managed by BGRI-MAS, represent desert grassland, dry steppe, and mountain grassland in Mongolia [7]. The fourth, the Baotou RadCalNet site in China, near Mongolia's desert grassland, provides calibration data for harmonizing remote sensing imagery [35, 36]. RadCalNet, including Baotou (China), La Crau (France), Railroad Valley (USA), and Gobabeb (Namibia), delivers automated surface reflectance measurements for sensor calibration, as shown in Figure 6 [35, 36].

Table 1. Geographical location of the sites

Site number	Site name	Location (decimal degree)
1	Desert grassland	45.73711 N, 108.7219 E
2	Dry grassland	47.67487 N, 112.407 E
3	Mountain grassland	48.17938 N, 108.4363 E
4	Baotou (BTCN) of RadCalNet, China	40.8658 N, 109.6155 E

Figure 6. The RadCalNet sites and the Baotou RadCalNet site, China (modified from [37]).

Chapter IV. DATA COLLECTION AND PREPROCESSING

This study utilized satellite and ground data for biomass monitoring [7, 17]. Satellite datasets comprised low-resolution JPSS-VIIRS, high-resolution PlanetScope SuperDove surface reflectance, Hyperspectral Hyperion EO-1 surface reflectance, and RSR data. Ground data included aboveground biomass, surface reflectance, and geolocation coordinates.

4.1 Aboveground Biomass

The aboveground dry biomass and geographic coordinates were measured by the BGRI-MAS team from 2020 to 2022 and jointly with Yamaguchi University in 2023 [7]. Wet biomass was collected from 85 1 m × 1 m plots using the hand-harvesting method at plant bases in desert grassland, dry steppe, and mountain grassland sites from 25 July to 10 August, coinciding with peak plant growth [7]. Table 2 summarizes biomass data, and Figure 7 illustrates the collection process. Hand-harvesting large areas is difficult, so plots were selected from homogeneous areas, independent of PlanetScope resolution, justifying the 1 m × 1 m size. Measurement locations were recorded using a handheld GPS [7]. In the field, all vegetation was harvested together due to challenges distinguishing green plants from litter. In the BGRI-MAS laboratory, green plants were separated from litter, and wet biomass was weighed before drying at 70°C for 72 hours (Figure 7c) [7]. Dry biomass was then weighed and expressed as grams per square meter (g/m²) [7].

Table 2. Ground biomass measurement numbers by year.

	2020	2021	2022	2023	Ground biomass measurement total number /2020 - 2023/
Desert grassland	7	6	8	12	33
Dry grassland	2	6	8	10	26
Mountain grassland	0	8	7	11	26
Total	13	20	23	33	85

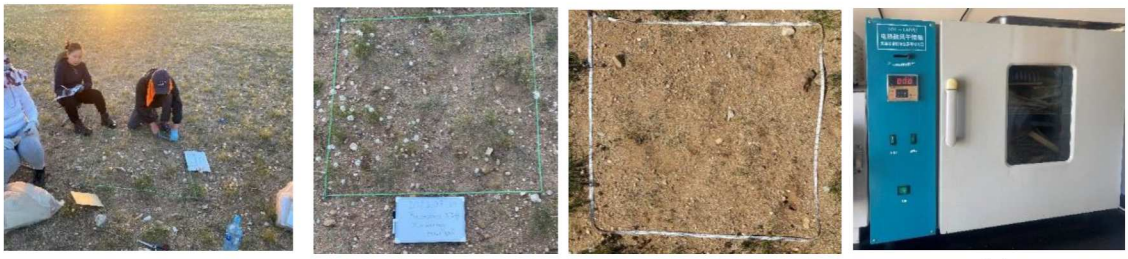

(a) (b (c)

Figure 7. Ground biomass measurement process in the desert grassland: (a) Measurement area (1m x 1m) before the harvest process, (b) measurement area after the harvest process, (c) drying process in the laboratory.

4.2 High-Resolution PlanetScope data

This study used 420 high-resolution PlanetScope images, with 343 for biomass estimation and grassland dynamic analysis (136 for mountain grassland, 107 for dry steppe, 100 for desert grassland) and 77 for evaluation of spectral harmonization [7, 17].

The PlanetScope constellation, comprising approximately 130 3U CubeSats (10 cm × 10 cm × 30 cm) in low-Earth, sun-synchronous orbits at 450–580 km altitude, captures daily nadir imagery of Earth's land surface [38]. Each satellite provides multiband images at 3.123–4.1 m spatial resolution with 12-bit radiometric resolution [38]. The constellation includes PS2.SD (Dove-R) and PSB.SD (SuperDove) instruments, selected for their similar blue, green, red, and near-infrared band wavelengths, offering four or eight spectral bands (Table 3) [38].

Table 3. PlanetScope Constellation and Sensor Specification.

Instrument	PS2 (July 2014 – April 2022)	PS2.SD (March 2019 – April 2022)	PSB.SD (March 2020 to current monitoring)
Orbit Altitude	475 km (~98° inclination)		
Equator Crossing Time	9:30 - 11:30 am (local solar time)		
Ground Sample Distance	3.7m (average at reference altitude 475 km)		
Spectral Bands	Blue: 455 - 515 nm Green: 500 - 590 nm Red: 590 - 670 nm NIR: 780 - 860 nm	Blue: 464 - 517 nm Green: 547 - 585 nm Red: 650 - 682 nm NIR: 846 - 888 nm	Coastal Blue 431-452 nm* Blue: 465-515 nm Green I: 513. - 549 nm Green II: 547. - 583 nm* Yellow: 600-620 nm* Red: 650 - 680 nm Red-Edge: 697 - 713 nm NIR: 845 - 885 nm
Pixel Size (orthorectified)		3.125 m	
Revisit time		Daily	
Bit Depth		Analytic (Radiance - W m-2 sr-1 μm-1): 16-bit Analytic SR (Surface Reflectance): 16-bit	
Atmospheric Corrections		Conversion to surface reflectance values using the 6SV2.1 radiative transfer code and MODIS NRT data. Reflectance values scaled by 10,000 to reduce quantization error.	

PlanetScope Ortho Tile and Scene images, processed as Level 3B BOA reflectance products, underwent radiometric and sensor corrections using the 6S radiative transfer code [39] and were stored as 16-bit TIFF files [38]. These images were acquired via the Planet Explorer platform (https://www.planet.com/explorer/). Satellite shown in Figure 8.

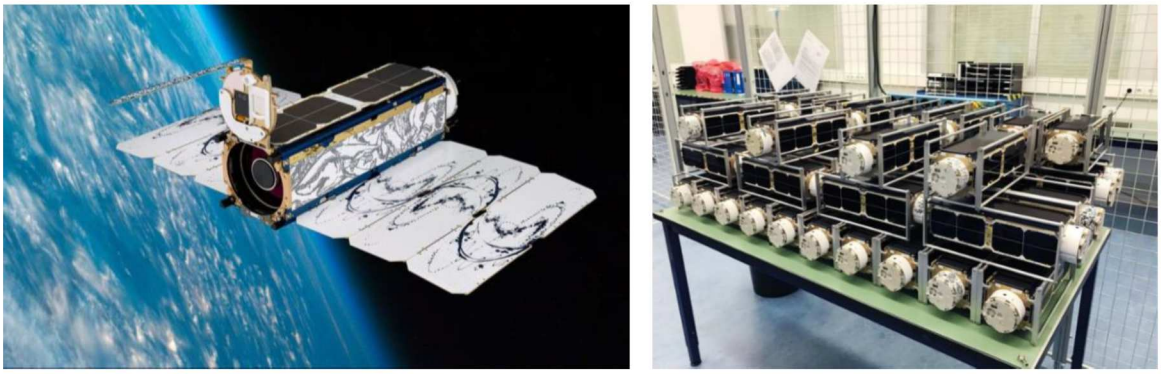

Figure 8. Physical images of a PlanetScope CubeSat.

4.2.1 Geographic Coordinates and Geometric Registration

Geographic coordinate measurements are indispensable when working with high-resolution (3-meter) satellite data, particularly given the small ground sampling area (1m x 1m for biomass and 3m x 3m for surface reflectance). Ensuring accurate matching of the geographic coordinates of ground sampling points with those of satellite image coordinates is vital for facilitating precise comparisons between ground and satellite images, thus significantly improving analysis accuracy. To achieve this, geometric registration was conducted for satellite images using the ground control point method, and the geographical coordinates of all measurement points were recorded.

During the study conducted across three sites (Figure 2) from July 20 to August 01, 2023, the geographic locations of all 149 measurements were meticulously recorded using handheld GPS Garmin Etrex20x instruments (Figure 9.a). These location measurements include three types of geographic coordinates: the first for the geo-location of biomass and surface reflectance measurement plots, the second for marking the geographic coordinates of fence corners and white sheet corners, and the third for measuring the distance between the measurement points.

For example, in Figures 9. b and 9. c, the biomass measurement point is marked in red, while orange, yellow, and green points present the satellite image geometric registration points.

The satellite image geometric registration process was carried out using the GCP method within the ENVI 5.6.2 software. In the grassland, challenges in locating ground control points led to the adoption of innovative methods in 2023, such as using white sheets sized 10m x 10m and 3m x 3m. In preceding years, fences and nearby objects like buildings within the research area served as ground control points. Geometric registration was performed on a total of 343 PlanetScope images during the study [7].

For instance, Figure 10 illustrates the geometric registration for a PlanetScope 3B-Scene image captured on August 1, 2023, over the study site of the dry grassland area. Figure 10.a presents

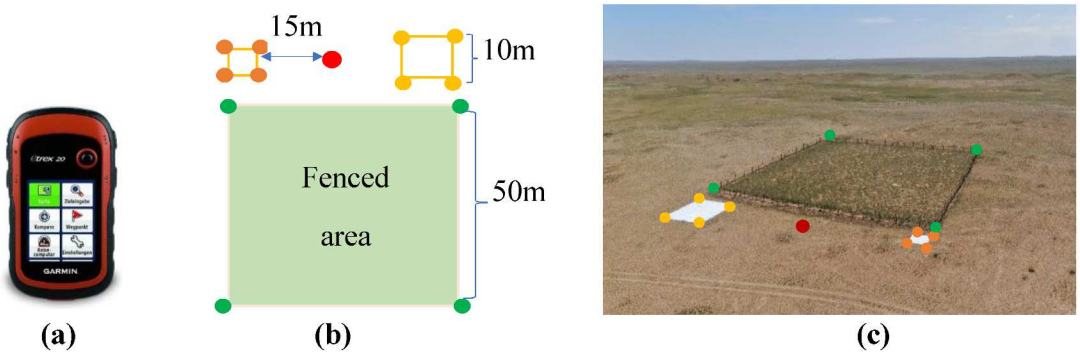

Figure 9. Geographic coordinate measurement: (a) Garmin Etrex 20x, (b) Measurement design showing green (fence corners), orange (3m x 3m white sheet), yellow (10m x 10m white sheet), and red (biomass measurement) points, (c) desert grassland research area image.

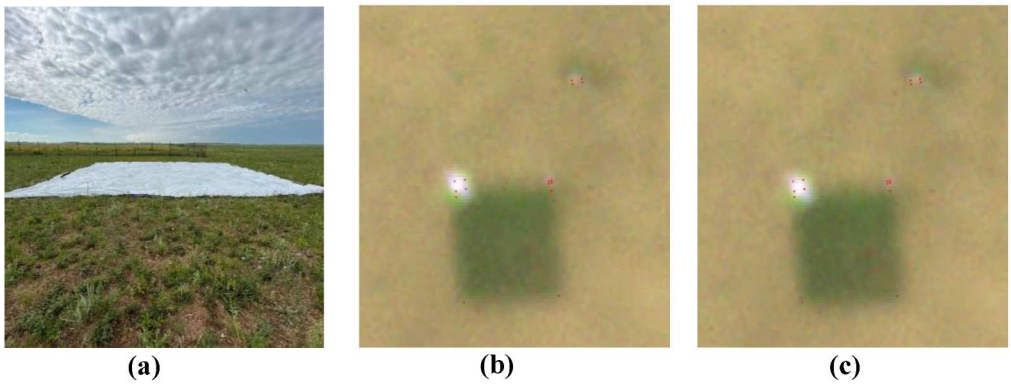

Figure 10. White sheet usage for geometric registration: (a) ground image in dry grassland, (b) PlanetScope image in dry grassland on August 01, 2023, (c) PlanetScope image of geometrically registered dry grassland on August 01, 2023.

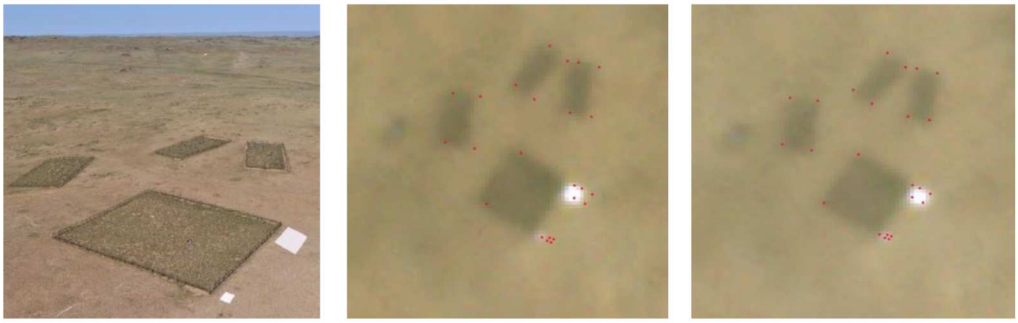

(a) (b) (c)

Figure 11. White sheet usage for geometric registration: (a) View of desert grassland field Ground image in desert grassland, (b) PlanetScope image in desert grassland on July 30, 2023, (c) PlanetScope image of geometrically registered desert grassland on July 30, 2023.

(a) (b (c)

Figure 12. (a) Ground image in Mountain grassland: (b) PlanetScope image in mountain grassland on August 01, 2023, (c) PlanetScope image of geometrically registered mountain grassland on August 01, 2023.

the field view, Figure 10.b displays the PlanetScope image before geometric registration, and Figure 10.c showcases the PlanetScope image after geometric registration. During this registration process, red points served as ground control points, with white sheets utilized explicitly for this purpose, resulting in a coordinate difference of 4.2 meters. Similar processes are depicted in Figure 11 for desert grassland and Figure 12 for mountain grassland, revealing coordinate differences between ground measurements and satellite images of 3.3 meters and 6 meters, respectively.

4.2.2 Surface Reflectance and Radiometric Correction

The PlanetScope level 3B images are already radiometrically corrected, and the bottom-of-atmosphere surface reflectance image products [38] have been utilized in this study.

However, we conducted additional radiometric correction by measuring surface reflectance in the research field area to enhance the accuracy assessment.

Spectral reflectance measurements were conducted at the three study sites (Figure 2) from July 26 to August 01, 2023, simultaneously with biomass data collection. An ASD FieldSpec HandHeld 2 Spectroradiometer (Figure 13.a) was utilized for measurements, with a wavelength range of 325 nm to 1025 nm and a field of view angle of 25 degrees [40].

The measurement design involved setting the measurement height 'h' at 1.2 meters and calculating the ground field area 'S' as 0.23 m² (Figure 13.b). In each plot, 16 measurements were conducted, and the average values of these measurements were used for correlation. The plot size of 3m x 3m closely matched the resolution of PlanetScope imagery (Figure 13.c). All measurements were taken between 10:00 AM and 12:00 PM to align with the timing of Planet satellite image capture. Measurements of a white reference panel (Spectralon plate, Labsphere Inc.) were taken immediately before each spectral reading. A total of 384 spectral measurements were obtained from 24 plot fields across the three study sites (Figure 13.d).

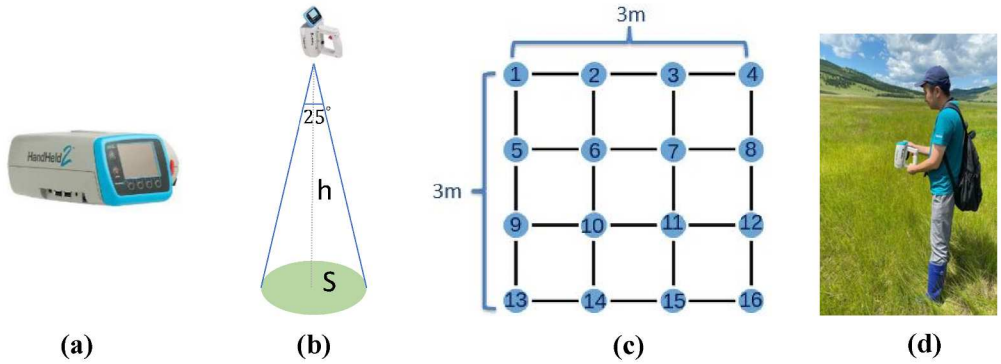

Figure 13. Surface reflectance measurement process: (a) ASD FieldSpec HandHeld2 spectroradiometer, (b) design of one measurement, (c) the measurement points in one plot, (d) measurement process in grassland.

PlanetScope PS2.SD and PSB.SD instrument images were used for this study, and their wavelength ranges are nearly identical (Table 3). Therefore, the same correction estimation method was applied to both of these instrument images.

The radiometric correction was carried out in two stages. First, all ground-measured surface reflectance was calculated for the Red and NIR band wavelength range of PlanetScope PS2.SD and PSB.SD instruments. Second, the PlanetScope surface reflectance value was

calculated from a 16-bit GeoTiff image by scaling 10,000 to a digital number [38]. All images were then converted to surface reflectance from the digital number using Equation (1).

$$SR_{planet} = DN_{planet} \times Scale \quad (1)$$

Where:

SRplanet – Surface Reflectance value of PlanetScope image

DNplanet – Digital Number of PlanetScope image

Scale – Scale factor from GeoTIFF image metadata. Equal to 0.0001.

After the conversation, a linear regression correlation method was applied to establish a correlation between ground surface reflectance and PlanetScope surface reflectance for separate Red and NIR bands. In this study, the NDVI was derived for AGB estimation. Therefore, corrections were conducted for the Red and NIR bands.

The resulting correlations for the grassland study area are shown in Figure 10, and the Red band has a correlation $R^2 = 0.9788$ and an NIR band $R^2 = 0.9728$, respectively.

These results indicate a strong relationship between PlanetScope surface reflectance and ground-measured surface reflectance, providing support for using Equation (2) for the Red band and Equation (3) for the NIR band of PlanetScope PS2.SD SDB.SD instruments image.

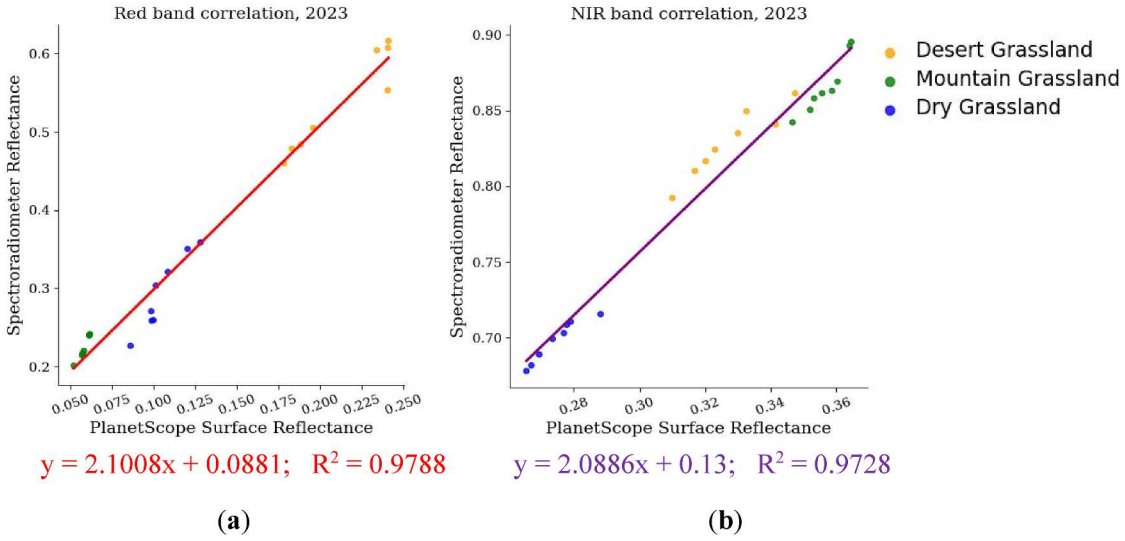

Figure 14. Correlation between field measurements and PlanetScope SR: (a) Red band correction, (b) NIR band correction.

$$y = 2.1008x + 0.0881 \quad (2)$$

$$y = 2.0886x + 0.13 \quad (3)$$

The correlation results from 2023, Equations (2) and (3), were also applied to biomass estimation of all satellite images.

4.3 Low-Resolution JPSS-VIIRS Data

The Joint Polar Satellite System (JPSS), developed by NOAA and NASA, is a next-generation polar-orbiting environmental satellite system. Its Visible Infrared Imaging Radiometer Suite (VIIRS), onboard the JPSS - Suomi NPP, JPSS1 - NOAA-20, and JPSS2 - NOAA-21 satellites, launched between 2011 and 2022, plays a vital role in global environmental monitoring and weather forecasting. VIIRS builds on the capabilities of AVHRR, MODIS, and SeaWiFS by observing clouds and Earth surface variables, while other instruments onboard focus on atmospheric and radiation measurements. With a field of view of 112.56°, VIIRS offers a swath width of 3060 km at an altitude of 829 km, providing full daily coverage of the Earth, both day and night. The instrument contains 22 spectral bands: 16 moderate-resolution bands (M-bands) with a 750 m spatial resolution at the nadir, five imaging bands (I-bands) with a 375 m spatial resolution, and a panchromatic Day/Night Band (DNB) with a 750 m resolution (Table 4) [17, 41].

(a) (b)

Figure 15. (a) JPSS satellite series overview, (b) image of JPSS-JPSS1.

Table 4. A characteristic of VIIRS Bands.

VIIRS band	Central wavelength (μm)	Wavelength range (μm)	Band explanation	Spatial resolution (m)
M1	0.412	0.402 - 0.422	Visible	750 m
M2	0.445	0.436 - 0.454		
M3	0.488	0.478 - 0.488		
M4	0.555	0.545 - 0.565		
M5 (B)	0.672	0.662 - 0.682		
M6	0.746	0.739 - 0.754	Near IR	
M7 (G)	0.865	0.846 - 0.885		
M8	1.240	1.23 - 1.25	Shortwave IR	
M9	1.378	1.371 - 1.386		
M10 (R)	1.61	1.58 - 1.64		
M11	2.25	2.23 - 2.28		
M12	3.7	3.61 - 3.79	Mediumwave IR	
M13	4.05	3.97 - 4.13		
M14	8.55	8.4 - 8.7	Longwave IR	
M15	10.763	10.26 - 11.26		
M16	12.013	11.54 - 12.49		
DNB	0.7	0.5 - 0.9	Visible	
I1 (B)	0.64	0.6 - 0.68	Visible	375 m
I2 (G)	0.865	0.85 - 0.88	Near IR	
I3 (R)	1.61	1.58 - 1.64	Shortwave IR	
I4	3.74	3.55 - 3.93	Mediumwave IR	
I5	11.45	10.5 - 12.4	Longwave IR	

For this study, 140 granules of VIIRS SDR data were collected over 35 days (September 1–7, 2020–2024) from NOAA's CLASS Archive [42] to map Mongolia. Approximately four granules per day were needed for complete coverage of the region, as shown in Figure 16. The SDR data, stored in Hierarchical Data Format version 5 (HDF5), contained non-gridded TOA

reflectance, radiance, and brightness temperature [41]. Preprocessing was essential to convert TOA reflectance to BOA surface reflectance and georeferencing [41].

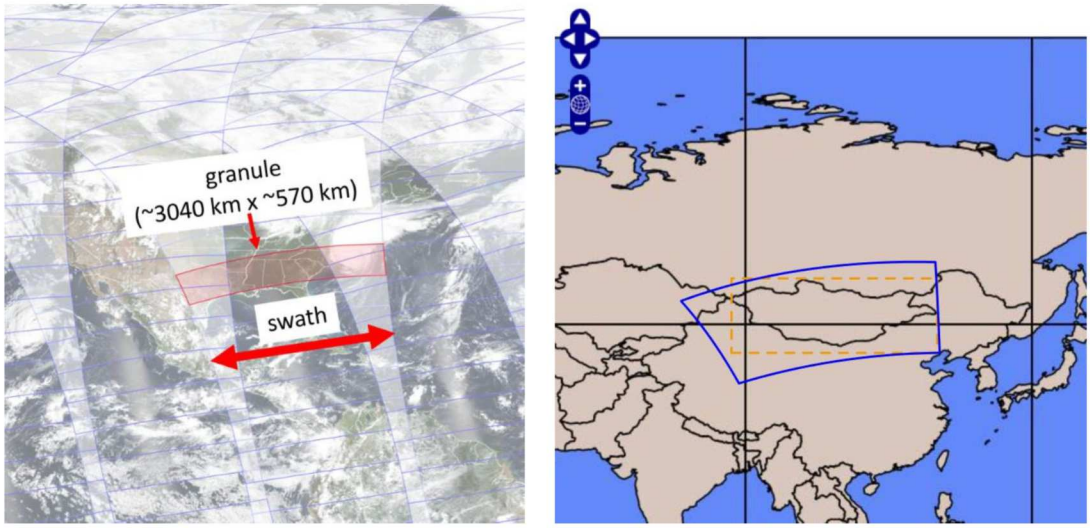

(a) (b)

Figure 16. The granule of VIIRS: (a) One VIIRS granule (from [42]), (b) data download process from NOAA Class [43].

3.1 Conversion of TOA Reflectance to BOA Reflectance and Georeferencing

The general preprocessing is illustrated in Figure 17, and the software workflow is detailed in Figure 19.

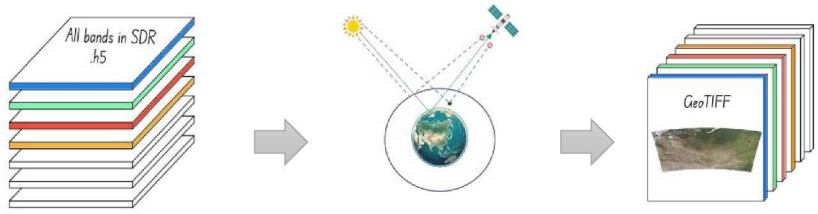

Figure 17. JPSS-VIIRS SDR Data Pre-Processing Diagram.

The Community Satellite Processing Package (CSPP), developed by the Space Science and Engineering Center at the University of Wisconsin-Madison, facilitates this preprocessing [44]. First, auxiliary data files, including cloud masks, cloud height, aerosol properties, and

weather prediction data, are generated using CSPP VIIRS ASCI V1.2 software with dynamic ancillary inputs [44]. Second, CSPP VIIRS Land Surface Reflectance software converts TOA to BOA reflectance, applying Lambertian atmospheric correction, adjacency adjustments to minimize surrounding pixel glare, and bidirectional reflectance distribution function (BRDF) coupling adjustments, leveraging the auxiliary data and SDR inputs [44, 45].

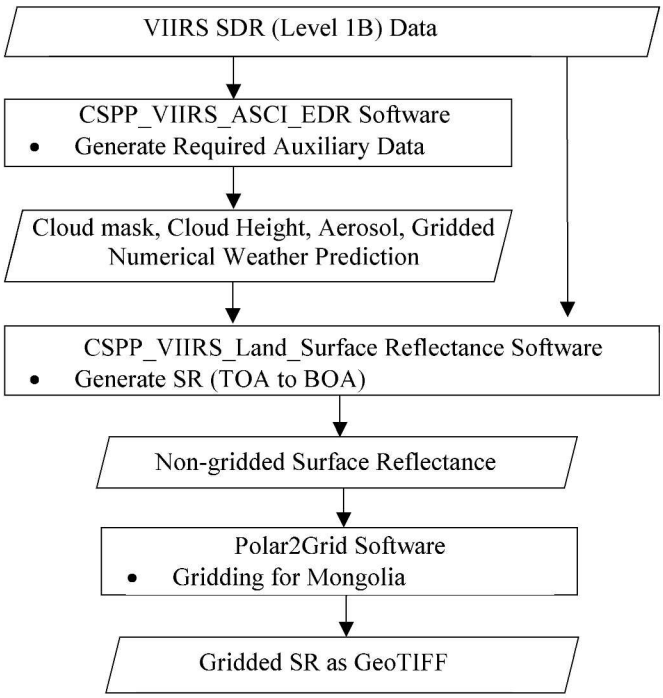

Figure 18. Preprocessing Flow Diagram for VIIRS SDR Data.

The Georeferencing required remapping to correct the VIIRS bow-tie effect, as shown in Figure 19 [41]. Remapping reorganizes satellite data into a consistent grid structure [44]. For this

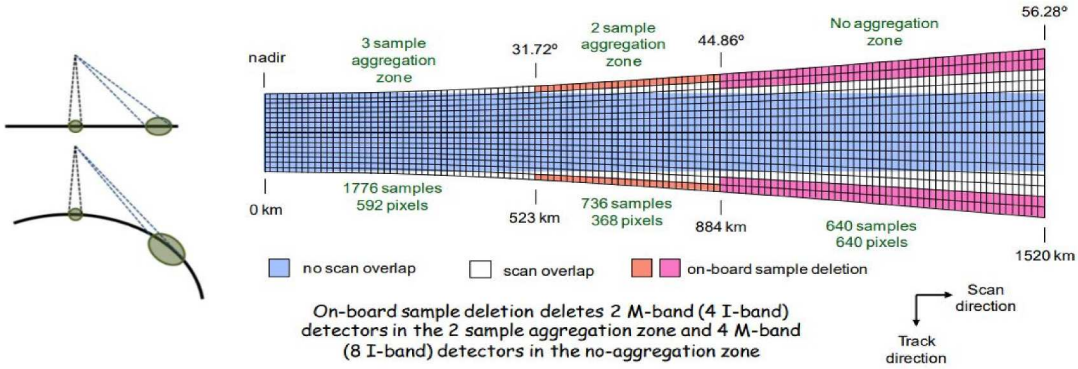

Figure 19. The VIIRS data bow-tie effect schematics, bow-tie deletion, and aggregation scheme for single-gain M-bands (from [41]).

study, nearest-neighbor remapping at a 375 m resolution was applied, targeting Mongolia, followed by projection to the WGS84 coordinate system (EPSG:4326) and export as GeoTIFF images using Polar2Grid V3.1 command-line tools [44]. This preprocessing ensures VIIRS SR for analysis and mapping.

4.4 Hyperspectral Hyperion EO-1

The Hyperion sensor aboard the Earth Observing-1 (EO-1) satellite, operational from 2000 to 2017, provides a unique archive for spectral libraries under real-world conditions. Hyperion captures data across 220 spectral bands (357 nm to 2.576 µm) with a spatial resolution of 30 m and a 7.7 km swath [46].

For this study, the Hyperion surface reflectance dataset, provided by the European Commission's Joint Research Centre, includes georeferenced and atmospherically corrected surface reflectance measurements from 10,000 points across various global surface types, as illustrated in Figure 20 [47][48]. This dataset serves as a valuable resource for surface reflectance analysis and was used for simulated surface reflectance to estimate the SBAF in spectral harmonization.

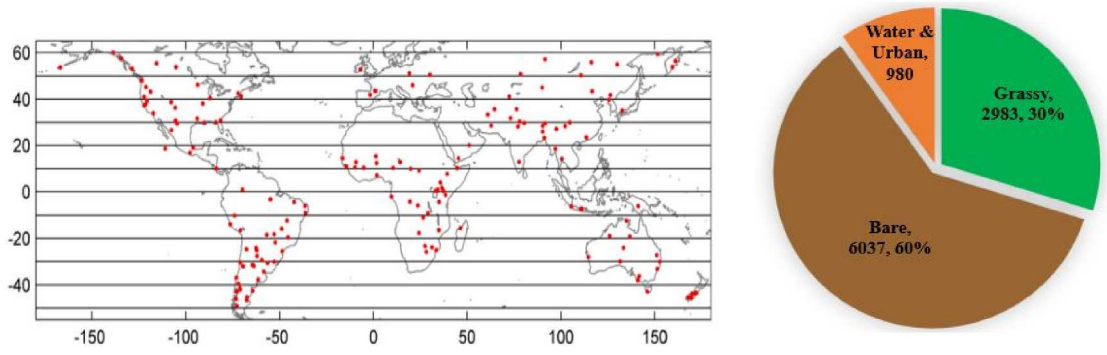

Figure 20. Map of the 158 Hyperion scenes used in this study and classification of the distribution of the 10,000 Hyperion spectra (modified from [48]).

4.5 Relative Spectral Response

The Relative Spectral Response (RSR) defines a satellite sensor's sensitivity to incoming radiation across different wavelengths. It is a crucial parameter that determines how a sensor detects and records spectral information. RSR is measured in a controlled laboratory environment before the satellite launch, where manufacturers use calibrated light sources and

detectors to characterize the spectral response of each sensor band. These pre-launch measurements ensure precise radiometric calibration and spectral accuracy for Earth observation applications [41].

This study analyzed the RSR data of VIIRS, PlanetScope SuperDove, and Hyperion EO-1 sensors to assess their spectral characteristics and compatibility for multi-sensor data integration. All sensor RSR data were downloaded from their official websites: VIIRS [49], PlanetScope [50], and Hyperion [51].

Figure 21 presents the RSR curves of the VIIRS, PlanetScope SuperDove, and Hyperion EO-1 sensors, illustrating their spectral band differences. Understanding these RSR differences is essential for spectral harmonization, ensuring consistent reflectance values when integrating data from multiple sensors.

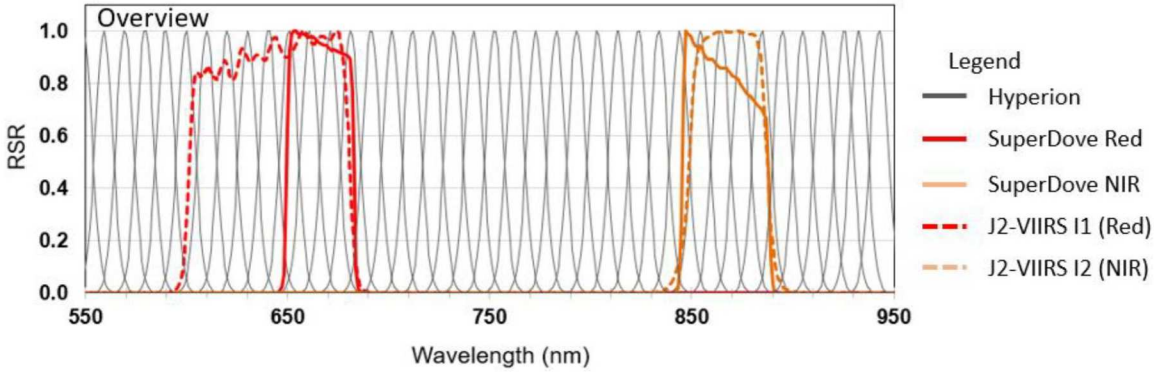

Figure 21. The graph of RSR.

Chapter V. MODEL DEVELOPMENT AND ADAPTATION

5.1 Model for Biomass Estimation utilizing PlanetScope data

This section outlines the formulation of a biomass estimation model using satellite data, serving as the initial step in developing a comprehensive monitoring framework for Mongolia's grasslands. The study employs high-resolution PlanetScope imagery to achieve precise biomass estimates, capturing fine-scale variations across diverse grassland types, such as desert, dry steppe, and mountain zones [7]. Specifically, this research marks the first application of PlanetScope imagery for estimating grassland biomass in Mongolia, aligning with understanding local grassland productivity and health outlined in Section 1.5. This model forms the foundation for subsequent adaptation to broader-scale monitoring [17].

Accurate biomass estimation is crucial and has been extensively explored. Biomass estimation models typically fall into two categories [5]: parametric models (e.g., linear, logarithmic, exponential, and other regression-based methods) [28, 52, 53], and non-parametric models (such as support vector machine (SVM), random forest (RF), and artificial neural network (ANN), which are part of machine learning) [54-57].

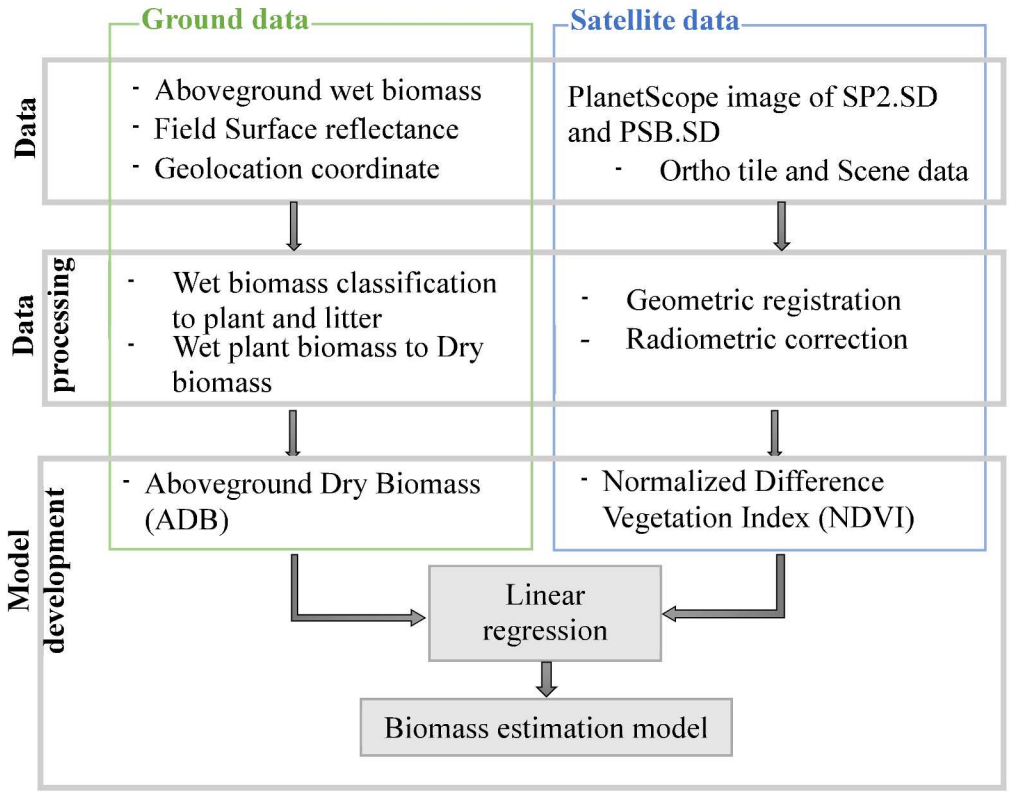

Figure 22. Flow diagram of biomass estimation model development.

One of our study objectives is to evaluate the accuracy of high-resolution PlanetScope imagery for biomass estimation in Mongolian grasslands. For this purpose, we chose the simple linear regression method because it relies solely on satellite data and is independent of additional parameters. This method establishes a relationship between above-ground dry biomass and the corrected PlanetScope NDVI. Specifically, the model utilizes a simple linear regression with only one regressor variable, as is characteristic of such models [34]. Figure 22 presents the methodology diagram for these biomass estimation model formulation steps.

The biomass estimation model utilized the simple linear regression method to establish a relationship between aboveground dry biomass and the corrected PlanetScope NDVI. The linear regression model with only one regressor variable is called a simple linear regression model [34].

The simple linear regression model is designed by Equation (4) [34].

$$Y = \beta_0 + \beta_1 X \quad (4)$$

Where Y is the dependent variable, X independent variable, β_0 is the intercept coefficient, β_1 is the slope coefficient.

The Normalized Difference Vegetation Index (NDVI) is calculated by Equation (5) [25, 26].

$$NDVI = \frac{NIR_{corrected} - Red_{corrected}}{NIR_{corrected} + Red_{corrected}} \quad (5)$$

For the modeling, 85 ground field measurement datasets (refer to Table 2) were employed during the growing season. The data were collected from May 2020 to September 2023 in desert and dry grasslands and from May 2021 to September 2023 in mountain grasslands. The corrected satellite data set was used for the estimation model as described in the geometric registration and radiometric correction section.

The commonly used statistical coefficient of determination in Equation (6) evaluates the model's quality [34, 58].

$$R^2 = 1 - \frac{\sum_{i=1}^{n}(y_i - \hat{y})^2}{\sum_{i=1}^{n}(y_i - \bar{y})^2} \quad (6)$$

Where i is the number of observations, y_i is the estimated variable, $\hat{y}$ is the average of the estimated variables, and $\bar{y}$ is the average of the predicted variables.

5.2 Model Adaptation to VIIRS data

This section describes the adaptation of a high-resolution biomass estimation model, originally developed using PlanetScope imagery, for use with daily VIIRS data via optimized spectral harmonization to support consistent and timely large-scale grassland biomass estimation.

5.2.1 Development of SBAF

The harmonization process applies the selected SBAF to VIIRS SR, adjusting red band reflectance to match PlanetScope's narrower range, validated against ground data from Mongolia [17]. Figure 23 illustrates how reflectance varies with grassland condition, underpinning the optimization approach. This step produces harmonized VIIRS SR compatible with the PlanetScope model, enabling biomass estimation at 375 m resolution.

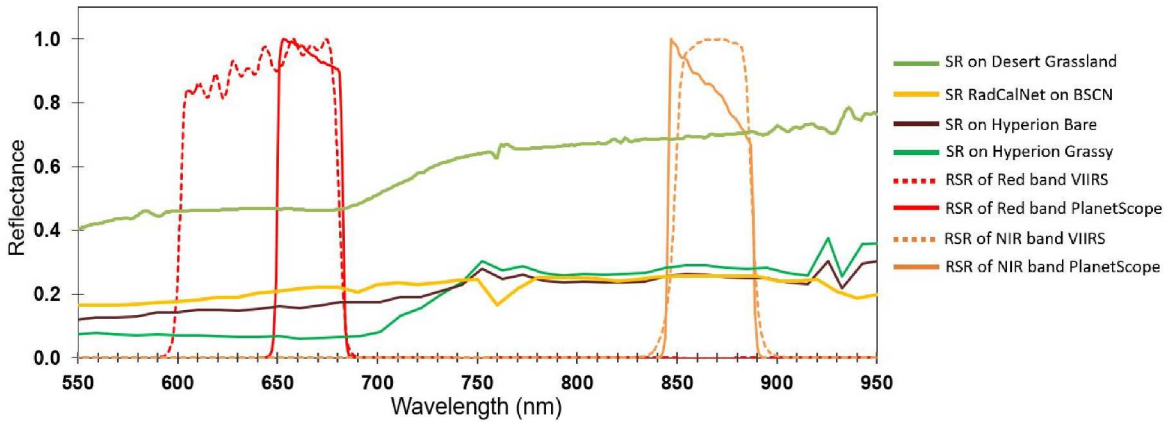

Figure 23. Graph of Surface Reflectance and RSR.

The development of SBAF follows the process outlined in Figure 24, which involves spectral harmonizing VIIRS SR with PlanetScope SR to minimize differences caused by variations in sensor RSR.

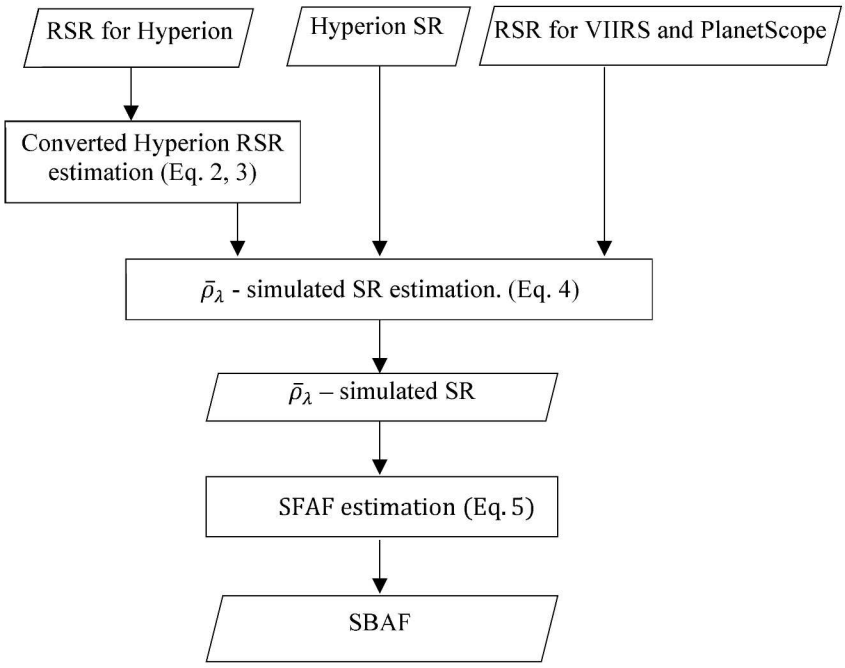

Figure 24. Flow Diagram of SBAF Estimation.

To simulate surface reflectance ($\bar{\rho}_\lambda$) for a satellite sensor's broader spectral band, hyperspectral surface reflectance (ρ_λ) was weighted according to the sensor's RSR and integrated over the bandpass (Equation (7)) [30, 45].

$$\bar{\rho}_\lambda = \frac{\int \rho_\lambda \times RSR_\lambda \times \Delta\lambda}{\int RSR_\lambda \times \Delta\lambda} \tag{7}$$

Hyperion's spectral bands encompass narrow wavelength (10nm) intervals, with the RSR exhibiting variation within these intervals following a non-linear function. The RSR is modeled (Equation (8)) using a Gaussian function, characterized by the average wavelength (μ) and the Full Width at Half Maximum (Equation (9)) [48, 59]:

Where σ is defined as:

$$RSR_\lambda = \frac{1}{\sigma\sqrt{2\pi}} e^{\frac{-(\lambda-\mu)^2}{2\sigma^2}} \tag{8}$$

$$\sigma = \frac{FWHM}{2\sqrt{2\log(2)}} \tag{9}$$

The integration of Hyperion's hyperspectral reflectance profile was calculated using the Hyperion reflectance (ρ_i), the sensor's RSR (RSR_b), and the relative spectral response of each Hyperion spectral band (RSR_H) (Equation (10)):

$$\bar{\rho}_b = \frac{\sum_i(\rho_i \int(RSR_{H,j}(\lambda) \times RSR_{b,j}(\lambda)\Delta\lambda))}{\sum_i(\int(RSR_{H,j}(\lambda) \times RSR_{b,j}(\lambda)\Delta\lambda))} \quad (10)$$

Where $\bar{\rho}_b$ is the simulated reflectance of spectral band b with the corresponding RSR (RSR_b), i – Hyperion spectral band, and j – RSR band range of Hyperion.

Once the band's simulated SR is identified, the SBAF is applied by Equation (11):

$$SBAF = \frac{\bar{\rho}_{\lambda(b\_tar)}}{\bar{\rho}_{\lambda(b\_ref)}} \quad (11)$$

Where $\bar{\rho}_{\lambda(b\_tar)}$ the simulated SR of the target sensor's band (VIIRS), $\bar{\rho}_{\lambda(b\_ref)}$ the simulated SR of the reference sensor's band (PlanetScope-SuperDove).

5.2.2 Optimization of SBAF for Grassland

This study focused on the Red and NIR bands, which are highly sensitive to vegetation reflectance. Due to broader spectral coverage in the VIIRS Red band (600–680 nm) compared to PlanetScope (650–680 nm), as illustrated in Table 5, greater variability was observed in reflectance, particularly in the Red band. As shown in Figure 23, grassy areas typically exhibit decreasing Red reflectance toward longer wavelengths, while bare areas show the opposite trend. This spectral behavior informed the optimization of SBAFs.

Table 5. PlanetScope Super-Dove and VIIRS sensors comparison.

Instrument	Red Band Range	NIR Band Range	Spatial Resolution	Revisit Time
PlanetScope SuperDove	650–680 nm	845–885 nm	3.125 meters	Daily
JPSS-2 VIIRS	600–680 nm	845–885 nm	375 meters	Daily

To address surface-specific variability, SBAFs were optimized by classifying reflectance conditions into three categories: grassy, bare, and sandy surfaces.

Grassy grassland: $NDVI \geq 0.3$ (VIIRS Red reflectance ≥ PlanetScope Red reflectance)

Bare grassland: $0.12 < NDVI < 0.3$ (VIIRS Red reflectance < PlanetScope Red reflectance)

Sand: $NDVI \leq 0.12$ (non-grassland)

The threshold *NDVI* values were derived by averaging *NDVI*, calculated as follows:

- Hyperion reflectance-based classification (grassy mean $NDVI_{grassy} \approx 0.568$ (3506 points), bare mean $NDVI_{bare} \approx 0.237$ (6494 points))
- Field-based observations (desert grassland $NDVI_{grassland} \approx 0.198$)
- RadCalNet sandy site ($NDVI_{sand} \approx 0.12$)

The classification threshold $NDV_{Hyperion}$ is 0.402 from the Hyperion SR:

$$NDVI_{hyperion} = \frac{NDVI_{grassy}+NDVI_{bare}}{2} = 0.402 \quad (12)$$

Finally, based on these NDVIs, the classification threshold $NDVI_{class}=0.3$ was calculated using Equation (13).

$$NDVI_{class} = \frac{NDVI_{Hyperion}+NDVI_{grassland}}{2} = 0.3 \quad (13)$$

The resulting optimization threshold of NDVI = 0.3 was used to assign optimized SBAFs to each pixel when harmonizing VIIRS data. This improved spectral alignment and model accuracy across grassland types.

5.2.3 Spectral and Radiometric Harmonization

The spectral harmonization of VIIRS imagery to PlanetScope imagery was conducted in the following steps, as illustrated in Figure 25. First, NDVI was estimated. Second, SBAF optimization was applied. Finally, SBAFs were applied for spectral harmonization. This process was implemented on a pixel-by-pixel basis.

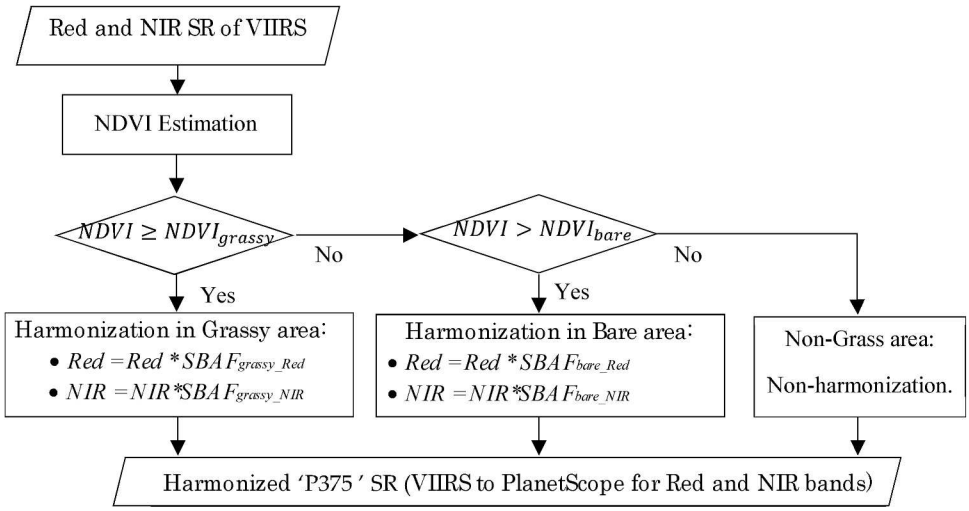

Figure 25. Flowchart of Spectral Harmonization.

Chapter VI. COMPUTATIONS

6.1 Biomass Estimations using PlanetScope and VIIRS

The developed model was utilized for biomass estimation with high-resolution PlanetScope and VIIRS imagery separately for three major Mongolian grassland types: desert grassland, dry grassland, and mountain grassland in selected small administrative units (Bags) across Mongolia (2020–2024) [7]. These 'Bag' areas also include the study sites of the research. Figure 4 illustrates the selected study area. Specifically:

- Desert Grassland: Olon-Ovoo Bag, Dalanjargalan soum, Dornogovi province (1610 km²)
- Dry Grassland: Lkhumbe Bag, Tumentsogt soum, Sukhbaatar province (1189 km²)
- Mountain Grassland: Jargalant Bag, Mungunmorit soum, Tuv province (1241 km²)

The quantitative and mapping analysis was conducted for these three grassland areas. The quantitative analysis enabled the uncertainty of model adaptation. The model adaptation uncertainty (VIIRS biomass estimation) was evaluated using statistical metrics, including RMSE, mean percentage difference, and coefficient of determination (R^2), to quantify the reliability of VIIRS-based biomass estimations under varying ecological conditions. The mapping analysis illustrated differences in pixels and estimations. This uniform mapping approach enables meaningful comparative analysis. We also created the histograms of predicted ADB for each map.

6.2 Time-Series Analysis of Grassland Dynamics in Grazed and Ungrazed Areas

Time series dynamic analyses of predicted ADB derived from PlanetScope satellite data were conducted for grazed and ungrazed areas across three grasslands in Mongolia from 2020 to 2023 [7]. These analyses focused on ADB dynamics during the vegetation growing season (May to September) over these four years. The ungrazed area is fenced off to protect it from animals and other human factors, facilitating comparative analysis with the grazed area. Another advantage is that grazed and ungrazed study areas are situated adjacent to each other, experiencing the same climate and weather conditions [7].

A total of 343 PlanetScope images were utilized for this analysis of three grassland areas. In this time series analysis, average values were calculated separately for four sampling points in ungrazed areas (orange points) and grazed areas (red points) across all images, as shown in Figure 26.

The average ungrazed biomass was calculated using the Equation (14):

$$Ungrazed\_Biomass = \frac{\sum_1^4 Ungrazed_{point(1-4)}}{4} \quad (14)$$

Where:

$Ungrazed_{point(1-4)}$ is ADB values for the four ungrazed sample points.

The average grazed AGB was calculated using Equation (15):

$$Grazed\_Biomass = \frac{\sum_1^4 Grazed_{point(1-4)}}{4} \quad (15)$$

Where:

$Grazed_{point(1-4)}$ is ADB values for the four grazed sample points.

The difference in ADB was calculated using Equation (16):

$$Difference\_Biomass = Ungrazed\_Biomass - Grazed\_Biomass \quad (16)$$

Where:

"*Ungrazed_Biomass*" is the average ADB value of the four ungrazed sample points.

"*Grazed_Biomass*" is the average ADB value of the four grazed sample points.

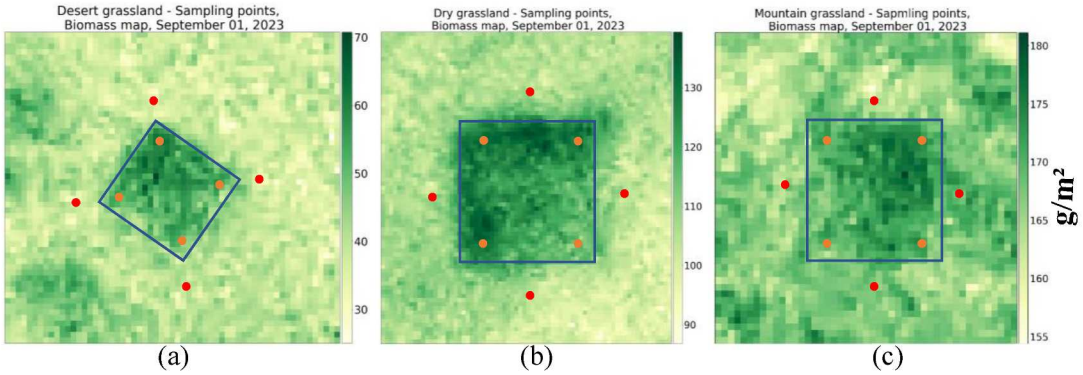

Figure 26. The predicted ADB for (a) desert grassland, (b) dry grassland, (c) mountain grassland, derived from PlanetScope on 01 September 2023.

6.3 Evaluation of Spectral Harmonization

The two spectral harmonization techniques, optimized SBAF and non-optimized SBAF, were evaluated using real satellite data. The evaluation compared VIIRS SR before SBAF implementation with harmonized P375 SR after applying SBAF, against PlanetScope SR, as illustrated in Figure 27.

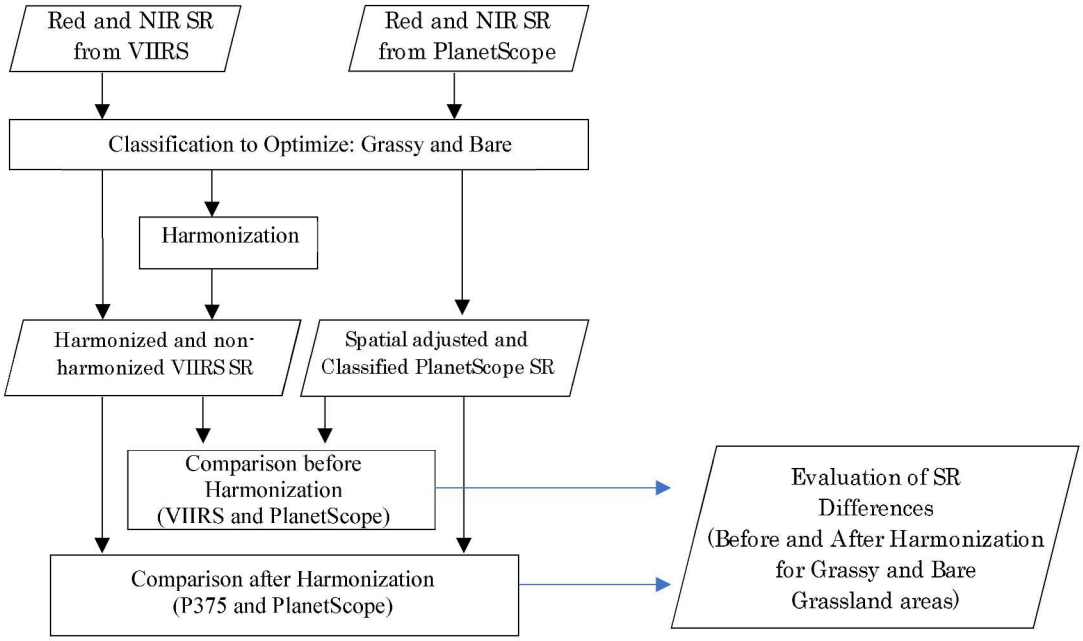

Figure 27. Flow chart of Spectral Harmonization Evaluation.

The evaluation was conducted on 593 grassland points in Mongolia during the first week of September (2023–2024), employing cloud-free imagery. Near-nadir points were selected for the VIIRS imagery to ensure optimal data quality.

To address differences in spatial resolution, spatial adjustment was performed. The VIIRS pixel resolution is 375 m, while the PlanetScope pixel resolution is 3.125 m. Therefore, the average value of 15,625 PlanetScope pixels (equivalent to one VIIRS pixel) was calculated. Before calculating the average, the centre coordinate of each VIIRS pixel was determined, and this coordinate was used as the reference for a centre location to estimate the PlanetScope average value.

6.4 Grassland Biomass Mapping Utilizing VIIRS Across Mongolia

Generating a biomass map for Mongolia using a single day of VIIRS data is impractical due to cloud cover. Instead, a maximum NDVI 7-day cloud-free mosaic approach was employed to create clear imagery. The following steps were applied to produce grassland biomass maps using VIIRS data:

- Harmonization and Corrections: Original VIIRS SR data were harmonized, and Sensor-specific adjustments were made to address radiometric discrepancies for grassland [7].
- NDVI Estimation: NDVI was calculated using corrected Red and NIR bands.
- Biomass Estimation: Biomass was then derived from the corrected NDVI, as shown in Equation (17).
- Map Generation: Final biomass and NDVI maps were produced. A water mask was applied to exclude water bodies and ensure a proper focus on grassland areas.

To ensure accurate mapping, maximum NDVI composites were created for each pixel over 35 days (September 1–7, 2020–2024). Daily NDVI values were computed, and the highest value within each 7-day window was selected, inherently excluding cloud-contaminated pixels due to their lower NDVI [60]. A water mask was applied to delineate water bodies, enhancing the accuracy of grassland mapping, spectral harmonization evaluation, and overall analysis [17]. This approach enables weekly biomass monitoring across Mongolia.

Chapter VII. RESULTS

7.1 Grassland Biomass Estimation

The PlanetScope data-driven biomass model was successfully developed, with results demonstrating that separate estimation models outperformed the combined model (section 7.1.1). This highlights the importance of grassland characteristics in biomass modeling. However, the combined model was selected to present the results. This choice aligns with the primary objective of creating an accurate and temporally consistent monitoring system for large-scale grassland areas, while also assessing the effectiveness of high-resolution data for Mongolia's grasslands. The model focused on aboveground biomass estimation across desert, dry, and mountain grasslands in the 'Bag' administrative units, utilizing PlanetScope and Harmonized VIIRS (P375) data [7, 17]. A comparative analysis shows the VIIRS biomass estimation uncertainty analysis (section 7.1.2).

7.1.1. Biomass Estimation Model

The biomass estimation model, developed using simple linear regression, correlates ADB measures from desert, dry, and mountain grasslands with PlanetScope NDVI. Equation (17) represents the predictive line, yielding an R-squared value of 0.6228 and an RMSE of 35.281 g/m², as illustrated in Figure 28 [7].

$$y = 309.72x + 8.5032 \quad (17)$$

where y is the predicted biomass, x is the corrected NDVI of PlanetScope.

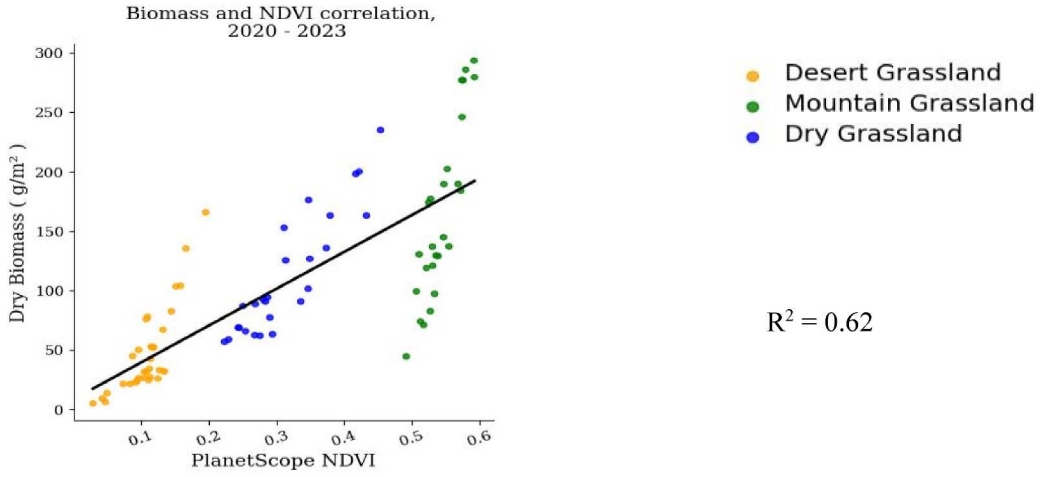

Figure 28. Correlation between field-measured ADB and calibrated PlanetScope NDVI.

Separate correlations between ADB and PlanetScope corrected NDVI were conducted for desert, dry, and mountain areas, and the regression lines are illustrated in Figure 28. The analysis of correlation gives a correlation coefficient of determination of 0.65 for desert grassland, 0.82 for dry grassland, and 0.80 for mountain grassland [7].

The outcome from the simple linear regression model suggests that separate modeling for grasslands yields better results than using a single common model [7].

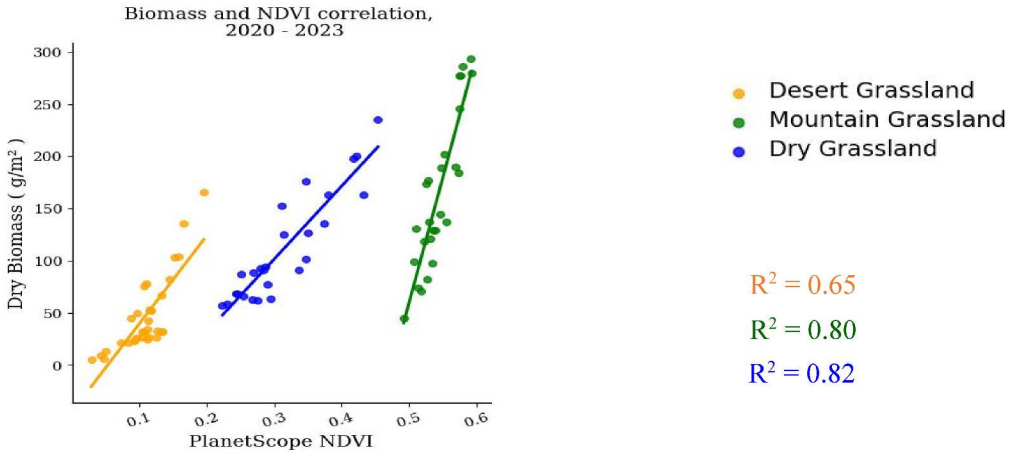

Figure 29. Correlation between field-measured ADB and calibrated PlanetScope NDVI, analyzed separately for three distinct areas.

7.1.2. Biomass Mapping Analysis

Biomass estimation maps for 2020–2024 were generated using the PlanetScope-based model and harmonized VIIRS (P375) data, covering Mongolia's desert, dry steppe, and mountain grasslands in 'Bag' units [7, 17]. PlanetScope maps, derived from high-resolution

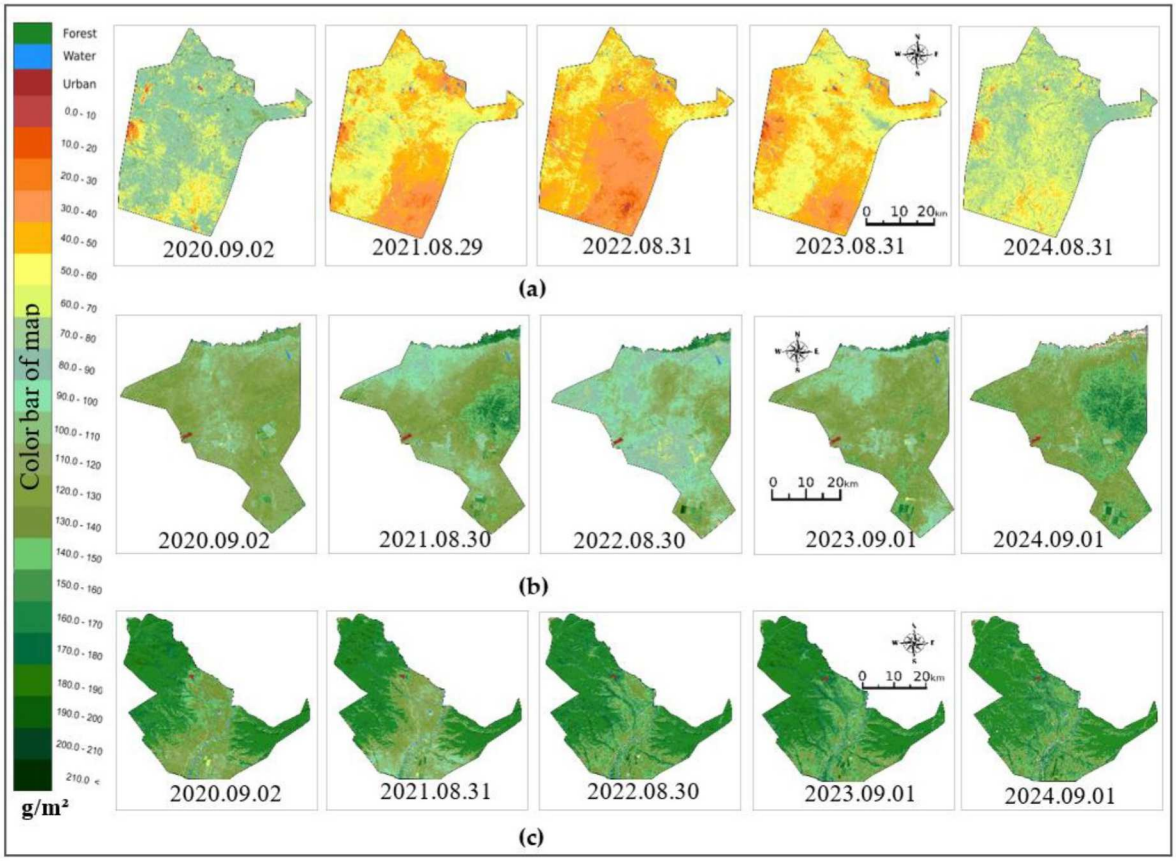

Figure 30. The predicted ADB across the desert grassland at Olon-Ovoo bag (a), the dry grassland at Lkhumbe bag (b), and the mountain grassland at Jargalant bag (c) derived from PlanetScope imagery.

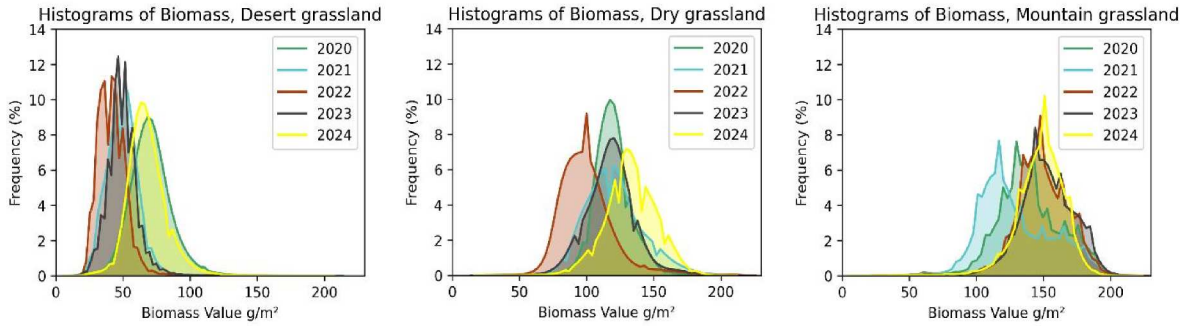

Figure 31. Histogram of predicted ADB maps derived from PlanetScope. (a) desert grassland images, (b) dry grassland images, and (c) mountain grassland images.

imagery, and P375 maps, spectral harmonized via SBAF, depicted ADB distributions for Olon-Ovoo Bag (desert grassland, Dalanjargalan Soum), Lkhumbe Bag (dry steppe, Tumentsogt Soum), and Jargalant Bag (mountain grassland, Mungunmorit Soum) [7]. Images from late August to early September were mapped consistently, with Figures 30 and 32 showing spatial biomass patterns and Figures 31 and 33 providing distribution histograms.

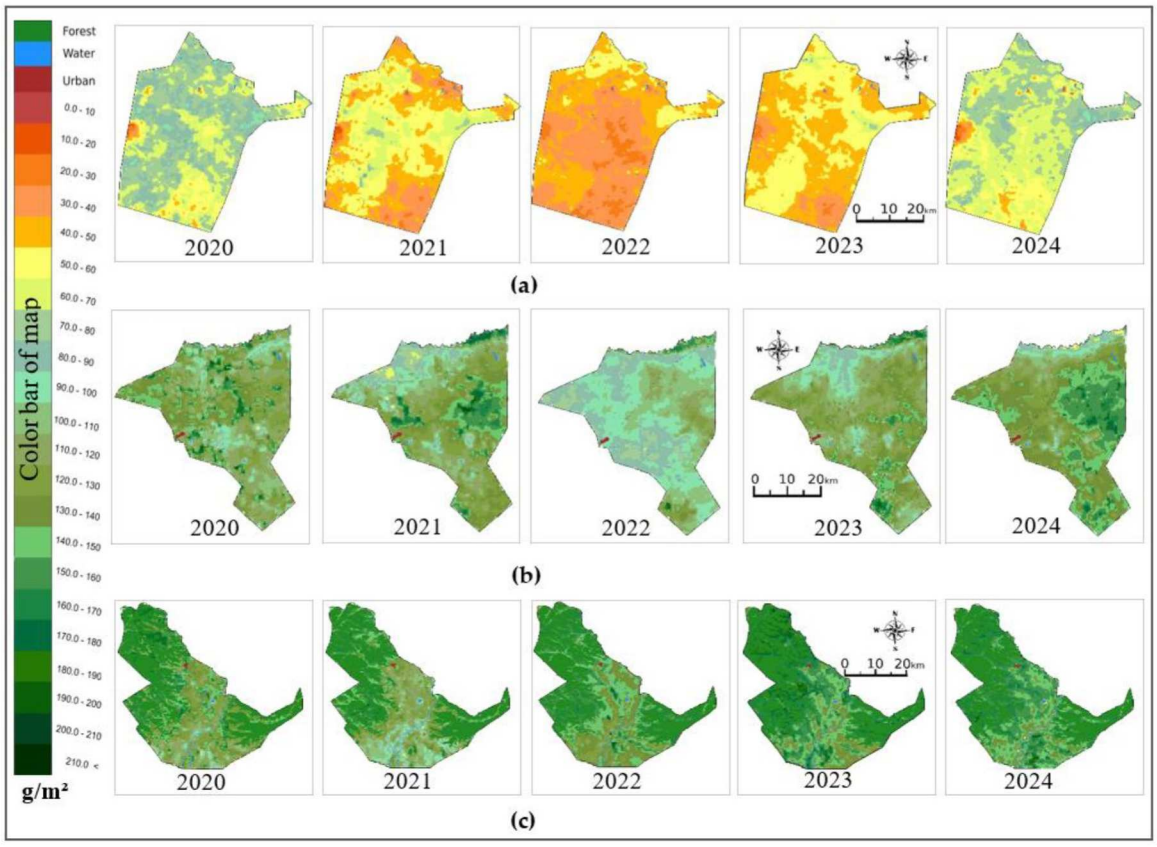

Figure 32. The predicted ADB across the desert grassland at Olon-Ovoo bag (a), the dry grassland at Lkhumbe bag (b), and the mountain grassland at Jargalant bag (c) derived from VIIRS imagery.

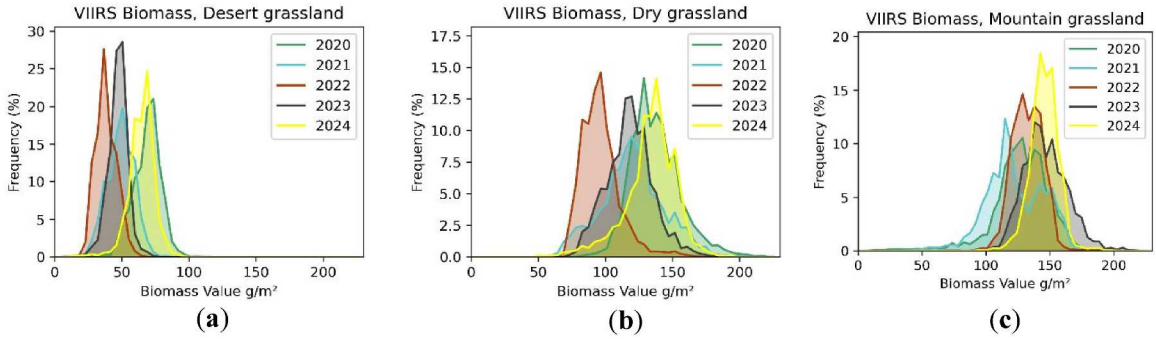

Figure 33. Histogram of predicted ADB maps derived from VIIRS. (a) desert grassland imagery, (b) dry grassland imagery, and (c) mountain grassland imagery.

Table 6 summarizes estimated ADB values. Mountain grasslands exhibited higher biomass than desert and dry steppe areas, reflecting ecological variations [7]. Field validation at BGRI-MAS sites confirmed the maps' consistency across grassland types [7].

PlanetScope estimates showed lower ADB in desert grassland (49 g/m²) compared to dry steppe (110 g/m²) and mountain grassland (136 g/m²), with peak values in 2024 and lower values in 2021–2022 [7]. P375 estimates were higher in desert (54 g/m², 10.5% difference) and dry steppe (122 g/m², 9.6% difference) but closely matched PlanetScope in mountain grassland (134 g/m², 1.9% difference) [17]. Figures 30–33 illustrate these trends, with sparse vegetation in desert areas driving larger discrepancies [7]. Mountain grasslands exhibited higher biomass, reflecting ecological variations [7].

Table 6. Predicted AGB for Bag areas.

Type	Instruments	Year					Average (g/m²)	Differences (%)
		2020	2021	2022	2023	2024		
Desert grassland	VIIRS (P375)	77 RMSE:12	54 RMSE:13	32 RMSE: 7	33 RMSE: 7	78 RMSE:13	54.8 RMSE: 10.04	10.5% (VIIRS > PlanetScope)
	PlanetScope	62 RMSE:15	41 RMSE:11	33 RMSE:10	40 RMSE:11	69 RMSE:14	49 RMSE: 12.2	
Dry grassland	VIIRS (P375)	142 RMSE:17	115 RMSE:23	92 RMSE:14	118 RMSE:16	146 RMSE:18	122.6 RMSE: 17.6	9.6% (VIIRS > PlanetScope)
	PlanetScope	110 RMSE:14	111 RMSE:21	91 RMSE:18	109 RMSE:18	133 RMSE:13	110.8 RMSE: 16.8	
Mountain grassland	VIIRS (P375)	138 RMSE:21	117 RMSE:22	129 RMSE:11	141 RMSE:16	145 RMSE:10	134 RMSE: 16	1.9% (VIIRS < PlanetScope)
	PlanetScope	131 RMSE:24	120 RMSE:27	140 RMSE:20	143 RMSE:20	149 RMSE:18	136.6 RMSE: 21.8	

Uncertainty evaluation compared P375 estimates to PlanetScope-derived values, yielding an RMSE of 11.6 g/m², a mean percentage difference of 10.74%, and an R^2 of 0.92 across all grasslands [17]. Mountain grasslands showed the lowest RMSE but limited variability, while desert and dry steppe displayed higher uncertainty due to ecological variability [7, 17].

7.2 Time Series Grassland Dynamic Analysis

Time-series dynamic analysis of ADB evaluated grazing impacts on Mongolia's grasslands from 2020 to 2023 [7]. Conducted at BGRI-MAS sites in Olon-Ovoo Bag (desert grassland, Dalanjargalan Soum), Lkhumbe Bag (dry steppe, Tumentsogt Soum), and Jargalant Bag (mountain grassland, Mungunmorit Soum), the analysis compared grazed and ungrazed plots to assess ecological trends [7]. Figures 34–36 show these trends, highlighting grazed-ungrazed differences that suggest potential grassland degradation from grazing pressures [7, 17]. Trends in grazed and ungrazed ADB, shown in Figures 34–36 for desert, dry steppe, and mountain grasslands, respectively, aligned with mapping results [7]. Desert grasslands exhibited strong growth in 2020 but reduced growth in 2022, while dry steppe and mountain grasslands showed steadier patterns [7]. Grazed-ungrazed ADB differences, indicated by red trend lines, increased over time, with slopes of 0.12 for desert grassland, 0.06 for dry steppe, and 0.03 for mountain grassland, reflecting stronger grazing impacts in desert areas [7, 34].

Increasing grazed-ungrazed differences, most pronounced in desert grasslands, suggest degradation linked to overgrazing and human activities [7]. Mountain grasslands showed stable trends, likely due to denser vegetation and lower grazing pressure [7]. These findings, validated by field data, demonstrate the multi-sensor approach's effectiveness in monitoring grassland dynamics across Mongolia's diverse ecosystems, supporting sustainable management [7].

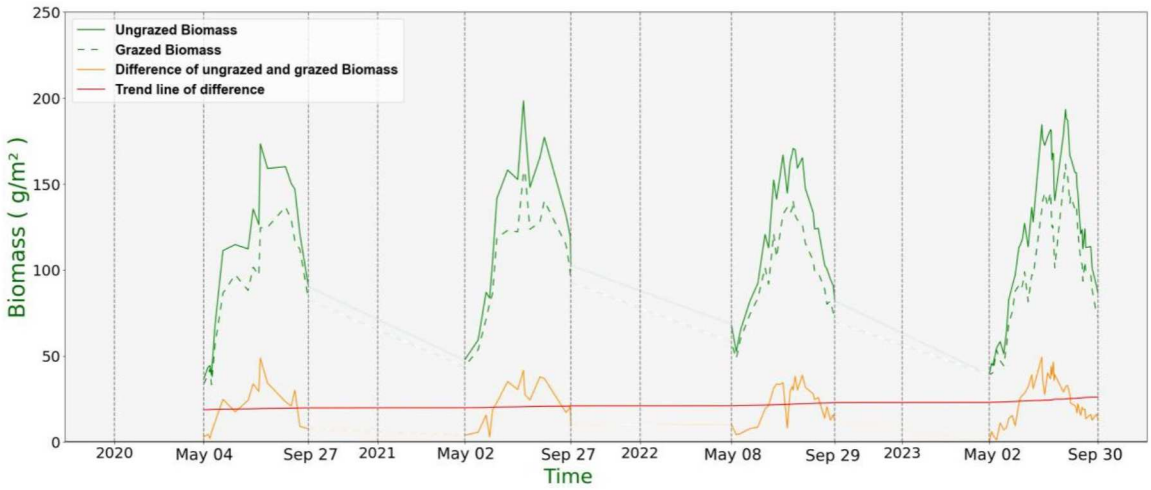

Figure 34. Time-series plot of predicted ADB and their differences, with trend lines, for ungrazed and grazed desert grassland areas during the growing seasons from May 2020 to September 2023.

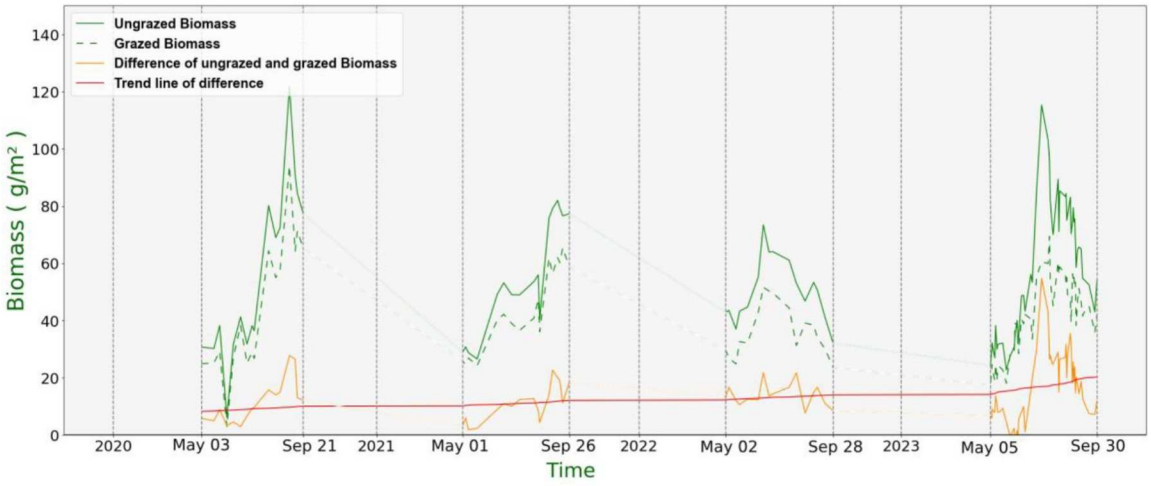

Figure 35. Time-series plot of predicted ADB and their differences, with trend lines, for ungrazed and grazed dry grassland areas during the growing seasons from May 2020 to September 2023.

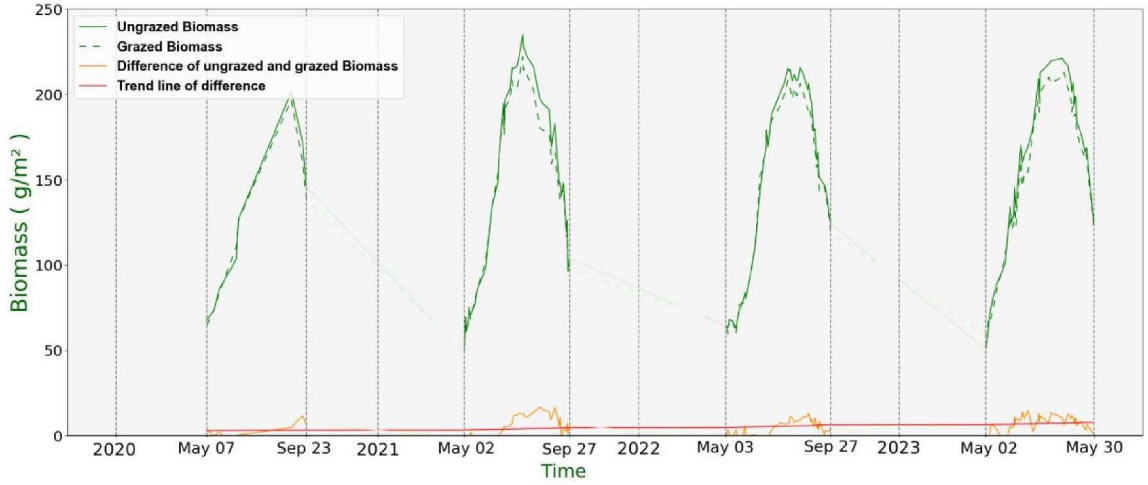

Figure 36. Time-series plot of predicted ADB and their differences, with trend lines, for ungrazed and grazed mountain grassland areas during the growing seasons from May 2020 to September 2023.

7.3 Accuracy Assessment of the Spectral Harmonization

Spectral harmonization aligned VIIRS and PlanetScope SR data using SBAFs derived for vegetated and bare areas in Red and NIR bands [7, 17]. Table 7 presents these SBAFs. Optimized and non-optimized SBAFs were compared to assess their effectiveness in reducing reflectance discrepancies [17]. The analysis utilized cloud-free imagery from early September

2023 and 2024, focusing on 593 grassland points across Mongolia, with near-nadir VIIRS imagery ensuring optimal quality [7].

Table 7. SBAFs for spectral harmonization from JPSS-VIIRS to PlanetScope-SuperDove.

Spectral Harmonization Approach \ Bands		SBAFs	
		Red	NIR
Optimized Harmonization	Grassy (440 point)	0.95	1.001
	Bare (153 point)	1.038	1.001
Non-optimized Harmonization (all 593 points)		1.008	1.001

Harmonization results showed reduced reflectance discrepancies, particularly in vegetated areas [17]. Before harmonization, notable differences appeared in the Red and NDVI bands. Optimized SBAFs decreased NDVI differences in vegetated areas from 5.5% to 3.1%, as shown in Figure 37 and Table 8 [17]. Bare areas exhibited smaller improvements, indicating better performance on vegetated surfaces [7]. Spatial alignment adjusted for resolution differences between VIIRS (375 m) and PlanetScope (3.125 m) [17].

Optimized SBAFs improved spectral compatibility between VIIRS and PlanetScope, especially in vegetated areas, enhancing biomass monitoring reliability [7, 17]. Bare areas showed persistent discrepancies, suggesting further SBAF refinement is needed [17]. These findings, validated across Mongolia's grasslands, highlight the multi-sensor approach's effectiveness for large-scale ecological monitoring, as detailed in Figure 37 and Tables 7 and 8 [7, 17].

Table 8. Evaluation of Spectral Harmonization.

Spectral Harmonization Approach \ Bands		Percentage Difference Before and After Spectral Harmonization					
		Red (%)		NIR (%)		NDVI (%)	
		Before	After	Before	After	Before	After
Optimized Harmonization	Grassy (440 point)	6.2	4.8	3.9	3.8	5.5	3.1
	Bare (153 point)	6.9	4	4.8	4.7	6.1	4.9
Non-optimized harmonization (all 593 points)		6.4	6.6	4.1	4.1	5.6	5.9

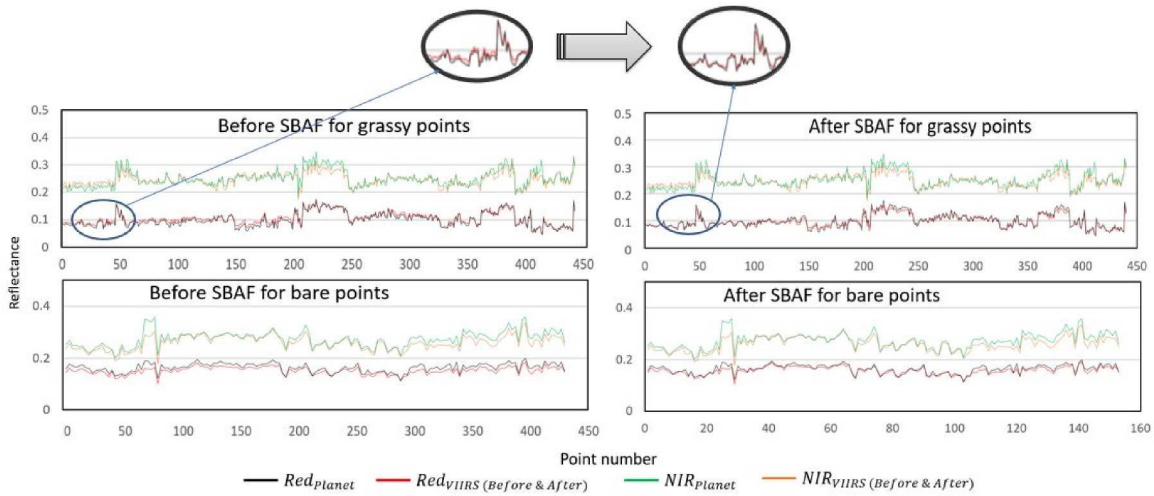

Figure 37. Comparison of PlanetScope and VIIRS SR before and after SBAF application: SR at grassy and bare points.

7.4 Grassland Biomass Mapping and Monitoring

Spectral harmonization facilitated VIIRS-based biomass estimation, and a 7-day maximum NDVI mosaic was created, yielding a clear image across Mongolia. These methods enable continuous weekly biomass mapping throughout the region, as illustrated in Figure 38, which presents an example of biomass mapping from September 1 to 7, 2024. This weekly mapping approach ensures consistent monitoring of Mongolia's grasslands. Figure 39 presents weekly biomass and NDVI maps, illustrating the spatial and temporal dynamics of ADB from 2020 to 2024 [7, 17].

The mapping results in Figure 39 highlight spatial variability and temporal changes in ADB [7]. The highest weekly average ADB was recorded in 2024 at 78 g/m², driven by favorable climatic conditions, while the lowest was in 2022 at 60 g/m², reflecting environmental stress [17]. Weekly averages for other years were 77 g/m² in 2020, 73 g/m² in 2021, and 69 g/m² in 2023 [7]. The five-year mean weekly ADB was 71.4 g/m² [7].

Weekly monitoring and the multi-sensor approach provided critical insights into climate-driven ecological trends, enabling the timely detection of biomass changes and supporting sustainable grassland management in Mongolia [7, 17].

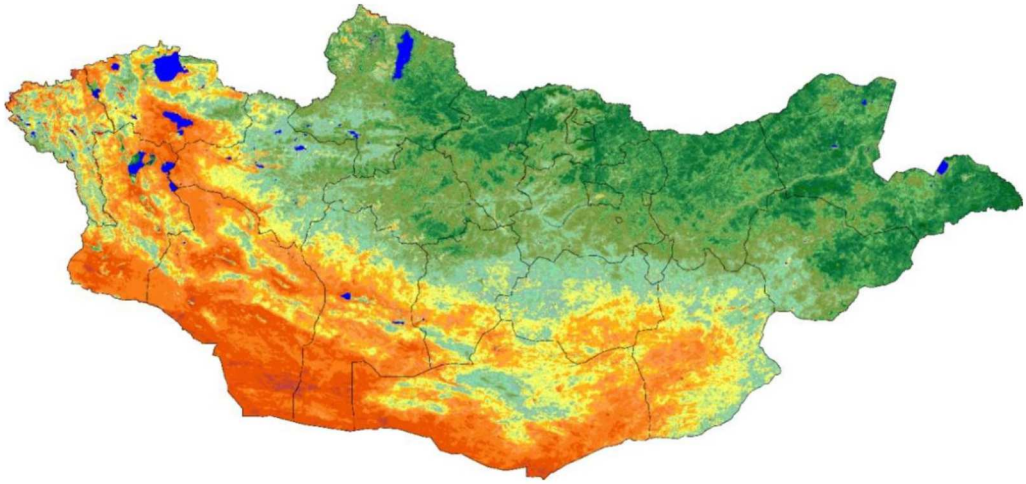

Figure 38. Predicted ADB map derived from VIIRS data, September 1–7, 2024.

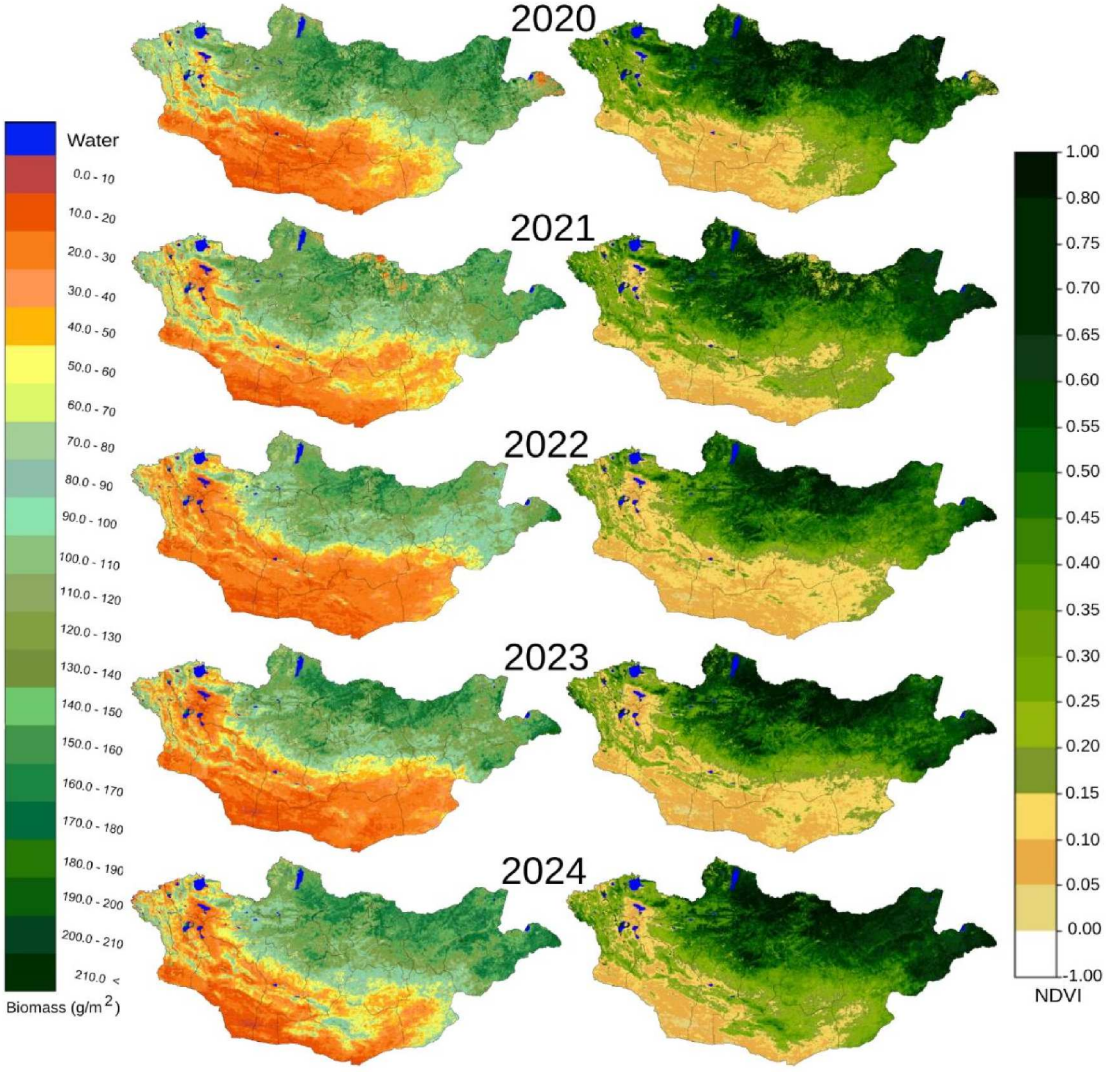

Figure 39. Predicted ADB and NDVI maps of Mongolia (September 1–7, 2020–2024).

Chapter VIII. DISCUSSION AND CONCLUSION

8.1 Discussion

This study pioneers a multi-satellite framework for grassland biomass monitoring in Mongolia, leveraging PlanetScope's high-resolution imagery (3.125 m) and VIIRS's daily coverage (375 m) to deliver precise and frequent assessments critical for ecological and socioeconomic sustainability. The PlanetScope-based model, employing simple linear regression with NDVI, achieved correlation coefficients (R^2) of 0.65, 0.82, and 0.80 for desert, dry, and mountain grasslands, respectively, with a combined R^2 of 0.62 and RMSE of 35.28 g/m². These results, while slightly below advanced models using Sentinel-2 or Landsat 8 ($R^2 \approx 0.75$, RMSE ≈ 20 g/m²) [13, 14], highlight PlanetScope's ability to capture fine-scale heterogeneity, particularly in desert grasslands, where radiometric corrections improved R^2 from 0.626 to 0.656. Time-series analysis (2020–2023) revealed significant biomass variability—e.g., desert grasslands dropped from 62 g/m² in 2020 to 33 g/m² in 2022—while grazed-ungrazed disparities (trend slopes: 0.12, 0.06, 0.03 for desert, dry, mountain) signaled ongoing degradation, aligning with reports of 58% grassland degradation nationally [8].

To better understand the drivers of inter-annual variability, we analyzed growing-season precipitation (May to September), which showed a strong correlation with biomass trends. Years with higher rainfall, such as 2021 (52.7 mm) and 2024 (49.1 mm), corresponded with increased biomass, while 2022, a notably dry year with only 33.4 mm of precipitation [8], had the lowest biomass across all grassland types. These findings highlight the importance of weather conditions, particularly precipitation, as a key driver of grassland productivity in Mongolia's semi-arid ecosystems.

To enable large-scale monitoring across Mongolia's 110.3 million hectares of pastureland, the PlanetScope model was adapted to VIIRS using an optimized SBAF, reducing red-band reflectance discrepancies from 6.2% to 4.8% in grassy areas ($NDVI \geq 0.3$) and 6.9% to 4.0% in bare areas ($0.12 < NDVI < 0.3$), with NDVI discrepancies dropping from 5.5% to 3.1% (grassy) and 6.1% to 4.9% (bare). The harmonized VIIRS data estimated a five-year average biomass of 71.4 g/m² (2020–2024), peaking at 78 g/m² in 2024 and dipping to 60 g/m² in 2022, with estimates of 54.8 g/m² (desert, +10.5% vs. PlanetScope), 122.6 g/m² (dry, +9.6%), and 134 g/m² (mountain, -1.9%). The overall accuracy (RMSE = 11.6 g/m², $R^2 = 0.92$, mean difference = 10.74%) confirms the approach's reliability, with mountain grasslands showing

the closest agreement due to their homogeneity, while desert and dry regions reflect greater ecological variability due to sparse vegetation and climatic fluctuations.

These findings have profound implications for stakeholders. For Mongolia's nomadic herders, comprising 26% of households [8], high-resolution biomass maps from PlanetScope enable optimized grazing, mitigating overgrazing in vulnerable desert grasslands. Policymakers can leverage VIIRS's weekly updates to prioritize conservation, supporting national efforts to address degradation [8, 11]. Globally, the methodology informs carbon sequestration monitoring, as grasslands cover 38% of Earth's terrestrial land [1], contributing to climate change mitigation. The integration of PlanetScope's spatial detail with VIIRS's temporal scalability offers a replicable model for semi-arid regions, enhancing remote sensing's role in sustainable land management. However, limitations include the PlanetScope model's reliance on NDVI, which constrained accuracy compared to multi-parameter models [7, 21, 32, 55, 61], and optical imagery issues such as cloud cover, which caused biomass fluctuations, possibly due to wet soil in desert grasslands in 2022 [7]. Ground surveys (85 plots, 1 m^2 across three sites) were precise but limited in scope, potentially missing regional variability [7], while VIIRS's coarser resolution introduced errors, notably a 10.5% discrepancy in desert grasslands [17]. The SBAF approach was less effective for non-vegetated areas (NDVI $\leq$ 0.12), and Hyperion's post-2017 unavailability restricted hyperspectral data [17, 43].

8.2 Conclusion

This dissertation establishes a robust multi-satellite framework for monitoring grassland biomass in Mongolia, synergizing PlanetScope's high-resolution imagery with VIIRS's frequent coverage to address ecological and socioeconomic challenges across 110.3 million hectares of pastureland. The PlanetScope model, using NDVI-based linear regression, delivered reliable biomass estimates (R^2 = 0.65, 0.82, 0.80 for desert, dry, mountain grasslands; combined R^2 = 0.62, RMSE = 35.28 g/m^2), capturing spatial variability—e.g., desert grasslands ranged from 62 g/m^2 (2020) to 33 g/m^2 (2022) [7, 17]. Dynamic analysis revealed increasing grazed-ungrazed disparities, with desert grasslands showing the fastest degradation (trend slope = 0.12), followed by dry (0.06) and mountain (0.03), corroborating national degradation concerns [7, 15, 16]. Adapting this model to VIIRS via an optimized SBAF enabled large-scale monitoring, reducing spectral discrepancies (e.g., red-band from 6.2% to 4.8% in grassy areas) and yielding a five-year biomass average of 71.4 g/m^2 (2020–2024), with 78 g/m^2 in 2024 and

60 g/m² in 2022. Estimates aligned closely with PlanetScope (RMSE = 11.6 g/m², R^2 = 0.92), varying by grassland type: 54.8 g/m² (desert), 122.6 g/m² (dry), 134 g/m² (mountain) [17]. This approach bridges resolution-frequency trade-offs, offering precise maps for herders to optimize grazing and frequent updates for policymakers to combat degradation. Globally, it supports carbon monitoring in grasslands, covering 38% of terrestrial land, and provides a scalable model for semi-arid ecosystems, advancing remote sensing for sustainable land management [1, 17].

Future research should enhance the biomass model by integrating multi-parameter inputs, such as soil moisture, Enhanced Vegetation Index, Green Chlorophyll Index, and machine learning methods (e.g., Random Forest, neural networks) to surpass current accuracy (R^2 = 0.62 to 0.82) [7, 23, 32, 55, 61]. Expanding ground surveys to cover more sites and incorporating Sentinel-2 data (10 m resolution) will improve validation across Mongolia's diverse grasslands [31]. Advanced harmonization with alternative hyperspectral sources like PRISMA [62] or AI-driven SBAF could minimize VIIRS discrepancies, particularly in desert grasslands (10.5% divergence) [17, 48]. Including year-round data, precipitation, livestock density, and other environmental factors will clarify degradation drivers [7]. Developing a near-real-time monitoring platform, delivering weekly biomass maps via cloud-based processing and mobile apps, could empower herders and inform dynamic policies for Mongolia's agencies [5, 17]. Extending this framework to other Central Asian grasslands will ensure resilience against climate and anthropogenic pressures, fostering data-driven sustainability to preserve Mongolia's pastoral heritage and support global grassland conservation [5, 7, 17].

References

1. White, R.S.; Murray, S.; Rohweder, M. *Pilot Analysis of Global Ecosystems Grassland Ecosystems;* World Resources Institute: Washington, DC, USA, 2000; pp. 1-6.
2. Pettorelli, N.; Safi, K.; Turner, W. Satellite remote sensing, biodiversity research and conservation of the future. *Philos. Trans. R. Soc.* B 2014, 369, 20130190. [CrossRef]
3. Liu, Y.; Hill, M.J.; Zhang, X.; Wang, Z.; Richardson, A.D.; Hufkens, K.; Filippa, G.; Baldocchi, D.D.; Ma, S.; Verfaillie, J.; et al. Using data from Landsat, MODIS, VIIRS and PhenoCams to monitor the phenology of California oak/grass savanna and open grassland across spatial scales. *Agric. For. Meteorol*. 2017, 237–238, 311–325. [CrossRef]
4. Herrero, M.; Thornton, P.K.; Gerber, P.; Reid, R.S. Livestock, livelihoods and the environment: Understanding the trade-offs. Curr. Opin. *Environ. Sustain*. 2009, 1, 111–120. [CrossRef]
5. Wang, Z.; Ma, Y.; Zhang, Y.; Shang, J. Review of Remote Sensing Applications in Grassland Monitoring. *Remote Sens*. 2022, 14, 2903. [CrossRef]
6. Reinermann, S.; Asam, S.; Kuenzer, C. Remote Sensing of Grassland Production and Management—A Review. *Remote Sens*. 2020, 12, 1949. [CrossRef]
7. Jargalsaikhan, M.-E.; Ichikawa, D.; Nagai, M.; Indree, T.; Katiyar, V.; Munkhtur, D.; Dashdondog, E. Aboveground Biomass Estimation and Time Series Analyses in Mongolian Grasslands Utilizing PlanetScope Imagery. *Remote Sens*. 2024, 16, 869. [CrossRef]
8. National Statistical Information Service. 2022. Mongolia Statistical Database. Available online: https://www.1212.mn/en (accessed on 22 April 2025).
9. Bonan, G. Ecological Climatology Concepts and Applications, 3rd ed.; Cambridge University Press: Cambridge, UK, 2016; p.367.
10. Tuvshintogtokh, I. The Steppe Vegetation of Mongolia; Bembi San: Ulaanbaatar, Mongolia, 2014; p. 7.

11. Paltsyn, M.Y.; Gibbs, J.P.; Iegorova, L.V.; Mountrakis, G. Estimation and Prediction of Grassland Cover in Western Mongolia Using MODIS-Derived Vegetation Indices. Rangel. Ecol. Manag. 2017, 70, 723–729. [CrossRef]

12. Garioud, A. Monitoring Grassland Dynamics by Exploiting Multi-Modal Satellite Image Time Series. Ph.D. Thesis, Gustave Eiffel University, Champs-sur-Marne, France, 2022.

13. Grassland Usage, 2022–2023. Available online: https://mofa.gov.mn/branch/maa (accessed on 22 April 2025).

14. Honeychurch, W. Inner Asia and the Spatial Politics of Empire: Archaeology, Mobility, and Culture Contact; Springer: New York, NY, USA, 2015.

15. United Nations Development Programme (UNDP). Mongolia's National Report on Desertification and Land Degradation; UNDP Mongolia: Ulaanbaatar, Mongolia, 2014. Available online: https://www.undp.org/mongolia/publications/national-report-desertification-and-land-degradation (accessed on 22 April 2025).

16. Munkhtsetseg, D.; Budbaatar, U.; Bulgamaa, D. National Report of the Grazing Impact Monitoring of Mongolia; Agency for Land Administration and Management Geodesy and Cartography: Ulaanbaatar, Mongolia, 2021. Available online: https://land.gov.mn/reports/grazing-impact-2021 (accessed on 22 April 2025).

17. Jargalsaikhan, M.-E.; Nagai, M.; Tumendemberel, B.; Dashdondog, E.; Katiyar, V.; Ichikawa, D. Adapting the High-Resolution PlanetScope Biomass Model to Low-Resolution VIIRS Imagery Using Spectral Harmonization: A Case of Grassland Monitoring in Mongolia. Remote Sens. 2025, 17, 1428. [CrossRef]

18. Lyu, X.; Li, X.; Gong, J.; Wang, H.; Dang, D.; Dou, H.; Li, S.; Liu, S. Comprehensive Grassland Degradation Monitoring by Remote Sensing in Xilinhot, Inner Mongolia, China. Sustainability 2020, 12, 3682. [CrossRef]

19. IPCC. Climate Change 2014: Synthesis Report; Intergovernmental Panel on Climate Change: Geneva, Switzerland, 2014. Available online: https://www.ipcc.ch/report/ar5/syr/ (accessed on 22 April 2025).

20. Henwood, W.D. Toward a strategy for the conservation and protection of the world's temperate grasslands. Great Plains Res. 2010, 20, 121–134.

21. Dashpurev, B.; Dorj, M.; Phan, T.N.; Bendix, J.; Lehnert, L.W. Estimating fractional vegetation cover and aboveground biomass for land degradation assessment in eastern Mongolia steppe: Combining ground vegetation data and remote sensing. *Int. J. Remote Sens*. 2023, 44, 452–468. [CrossRef]

22. Agency for Land Administration and Management, Geodesy, and Cartography. Land Monitoring Unit Responsibilities. Available online: https://old.gazar.gov.mn/p/suur-sudalgaa-monitoringijn-heltes (accessed on 23 April 2025).

23. Meng, B.P.; Liang, T.G.; Yi, S.H.; Yin, J.P.; Cui, X.; Ge, J.; Hou, M.J.; Lv, Y.Y.; Sun, Y. Modeling Alpine Grassland Above Ground Biomass Based on Remote Sensing Data and Machine Learning Algorithm: A Case Study in East of the Tibetan Plateau, China. IEEE J. Sel. Top. Appl. Earth Obs. Remote Sens. 2020, 13, 2986–2995. [CrossRef]

24. Gao, T.; Xu, B.; Yang, X.C.; Jin, Y.X.; Ma, H.L.; Li, J.Y.; Yu, H.D. Using MODIS time series data to estimate aboveground biomass and its spatio-temporal variation in Inner Mongolia's grassland between 2001 and 2011. Int. J. Remote Sens. 2013, 34, 7796–7810. [CrossRef]

25. Rouse, W., Jr.; Haas, R.H.; Well, J.A.; Deering, D.W. Monitoring Vegetation System in the Great Plains with ERTS. In Proceedings of the Goddard Space Flight Center 3d ERTS-1 Symposium, Washington, DC, USA, 1 January 1974.

26. Huete, A.; Didan, K.; Miura, T.; Rodriguez, E.P.; Gao, X.; Ferreira, L.G. Overview of the radiometric and biophysical performance of the MODIS vegetation indices. Remote Sens. Environ. 2002, 83, 195–213. [CrossRef]

27. Xu, D.; Chen, B.; Yan, R.; Yan, Y.; Sun, X.; Xu, L.; Xin, X. Quantitative monitoring of grazing intensity in the temperate meadow steppe based on remote sensing data. Int. J. Remote Sens. 2018, 40, 2227–2242. [CrossRef]

28. Edirisinghe, A.; Hill, M.J.; Donald, G.E.; Hyder, M. Quantitative mapping of pasture biomass using satellite imagery. Int. J. Remote Sens. 2011, 32, 2699–2724. [CrossRef]

29. Gao, F.; Masek, J.; Schwaller, M.; Hall, F. On the blending of the Landsat and MODIS surface reflectance: Predicting daily Landsat surface reflectance. IEEE Trans. Geosci. Remote Sens. 2006, 44, 2207–2218. [CrossRef]

30. Chander, G.; Mishra, N.; Helder, D.L.; Aaron, D.B.; Angal, A.; Choi, T.; Xiong, X.; Doelling, D.R. Applications of spectral band adjustment factors (SBAF) for cross-calibration. IEEE Trans. Geosci. Remote Sens. 2013, 51, 1267–1281. [CrossRef]

31. Claverie, M.; Ju, J.; Masek, J.G.; Dungan, J.L.; Vermote, E.F.; Roger, J.-C.; Skakun, S.V.; Justice, C. The Harmonized Landsat and Sentinel-2 surface reflectance data set. Remote Sens. Environ. 2018, 219, 145–161. [CrossRef]

32. Ramoelo, A.; Cho, M.A.; Mathieu, R.; Madonsela, S.; van de Kerchove, R.; Kaszta, Z.; Wolff, E. Monitoring grass nutrients and biomass as indicators of rangeland quality and quantity using random forest modelling and WorldView-2 data. Int. J. Appl. Earth Obs. Geoinf. 2015, 43, 43–54. [CrossRef]

33. Ren, Y.; Wen, Q.; Xi, F.; Ge, X.; Yuan, Y.; Hu, B. Monitoring Grassland Growth Based on Consistency-Corrected Remote Sensing Image. Remote Sens. 2023, 15, 2066. [CrossRef]

34. Montgomery, D.C.; Peck, E.A.; Vining, G.G. Introduction of Linear Regression Analysis; John Willey & Sons, Inc.: New York, NY, USA, 2021; pp. 1–5.

35. RadCalNet. (n.d.). Radiometric Calibration Network Database. Retrieved from https://www.radcalnet.org/#!/ (accessed on 15 December 2024).

36. Bouvet, M.; Thome, K.; Berthelot, B.; Bialek, A.; Czapla-Myers, J.; Fox, N.P.; Goryl, P.; Henry, P.; Ma, L.; Marcq, S.; et al. RadCalNet: A Radiometric Calibration Network for Earth Observing Imagers Operating in the Visible to Shortwave Infrared Spectral Range. Remote Sens. 2019, 11, 2401. [CrossRef]

37. Available online: https://ceos.org/home-2/wgcv-radcalnet/ (accessed on 03 Feb, 2025)

38. Planet.com. PlanetScope Product Specifications. 2022. Available online: https://assets.planet.com/docs/Planet_PSScene_Imagery_Product_Spec_letter_screen.pdf (accessed on 10 January 2023).

39. Vermote, E.; Tanré, J.D.; Deuzé, L.; Herman, M.; Morcrette, J.J.; Kotchenova, S.Y. Second Simulation of Satellite Signal in the Solar Spectrum-vector (6SV). 2006. Available online: https://gsweb11.umd.edu/files/6S/6S_Manual_Part_1.pdf (accessed on 29 December 2023)

40. ASD FieldSpec® HandHeld 2 User Manual. 2010, pp. 1–140. Available online: http://www.geo-informatie.nl/courses/grs60312/material2017/manuals/600860-Dhh2manual.Pdf (accessed on 10 July 2021).

41. Cao, C.; Xiong, X.; Wolfe, R.; DeLuccia, F.; Liu, Q.; Blonski, S.; Lin, G.; Nishihama, M.; Pogorzala, D.; Oudrari, H.; et al. Visible Infrared Imaging Radiometer Suite (VIIRS) Sensor Data Record (SDR) User's Guide; Version 1.3; NOAA Technical Reports, Washington, DC, USA, 2017. Available online: https://ncc.nesdis.noaa.gov/documents/documentation/viirs-users-guide-tech-report-142a-v1.3.pdf (accessed on 30 December 2024).

42. Available online: https://www.star.nesdis.noaa.gov/atmospheric-composition-training/satellite_data_viirs_granules.php (accessed on 01 Jan 2025).

43. Available online: https://www.aev.class.noaa.gov/saa/products/welcome (accessed on 25 March 2025).

44. Community Satellite Processing Package. Available online: https://cimss.ssec.wisc.edu/cspp/ (accessed on 16 February 2025).

45. Vermote, E.; Franch, B.; Roger, J.C.; Csiszar, I. Viirs Surface Reflectance Algorithm Theoretical Basis Document Version 3.0. Available online: https://www.ospo.noaa.gov/Products/land/sr/docs/VIIRS_SR_ATBD.pdf (accessed on 7 January 2025).

46. Available online: https://www.usgs.gov/centers/eros/science/usgs-eros-archive-earth-observing-one-eo-1-hyperion (accessed on 27 December 2024).

47. Available online: https://data.jrc.ec.europa.eu/dataset/6c90c9f0-e355-4eb2-9890-13244f9a5d99 (accessed on 7 January 2025).

48. Martin, C. Evaluation of surface reflectance bandpass adjustment techniques. ISPRS J. Photogrammetry and Remote Sens. 2023, 198, 210–222. [CrossRef]

49. Available online: https://ncc.nesdis.noaa.gov/NOAA-21/J2VIIRS_SpectralResponseFunctions.php (accessed on 7 January 2025)

50. Available online: https://support.planet.com/hc/en-us/articles/360014290293-Do-you-provide-Relative-Spectral-Response-Curves-RSRs-for-your-satellites (accessed on 7 January 2025).

51. Available online: https://www.eoportal.org/satellite-missions/eo-1#eop-quick-facts-section (accessed on 10 September 2023).

52. Edirisinghe, A.; Clark, D.; Waugh, D. Spatio-temporal modeling of biomass of intensively grazed perennial dairy pastures using multispectral remote sensing. Int. J. Appl. Earth Obs. Geoinf. 2012, 16, 5–16. [CrossRef]

53. Chu, D. Aboveground biomass estimates of grassland in the north Tibet using modies remote sensing approaches. Appl. Ecol. Environ. Res. 2020, 18, 7655–7672. Available online: https://aloki.hu/pdf/1806_76557672.pdf (accessed on 27 December 2023).

54. Zhang, B.; Zhang, L.; Xie, D.; Yin, X.; Liu, C.; Liu, G. Application of Synthetic NDVI Time Series Blended from Landsat and MODIS Data for Grassland Biomass Estimation. Remote Sens. 2016, 8, 10. [CrossRef]

55. Ramoelo, A.; Cho, M.A.; Mathieu, R.; Madonsela, S.; van de Kerchove, R.; Kaszta, Z.; Wolff, E. Monitoring grass nutrients and biomass as indicators of rangeland quality and quantity using random forest modeling and WorldView-2 data. Int. J. Appl. Earth Obs. Geoinf. 2015, 43, 43–54. [CrossRef]

56. Yang, S.X.; Feng, Q.S.; Liang, T.G.; Liu, B.K.; Zhang, W.J.; Xie, H.J. Modeling grassland above-ground biomass based on artificial neural network and remote sensing in the Three-River Headwaters Region. Remote Sens. Environ. 2018, 204, 448–455. [CrossRef]

57. Xie, Y.; Sha, Z.; Yu, M.; Bai, Y.; Zhang, L. A comparison of two models with Landsat data for estimating above-ground grassland biomass in Inner Mongolia, China. Ecol. Model. 2009, 220, 1810–1818. [CrossRef]

58. Richter, K.; Hank, T.B.; Mauser, W.; Atzberger, C. Derivation of Biophysical Variables from Earth Observation Data: Validation and Statistical Measures. J. Appl. Remote Sens. 2012, 6, 063557. [CrossRef]

59. Kim, Y., Huete, A. R., Miura, T., & Jiang, Z. (2010). Spectral compatibility of vegetation indices across sensors: Band decomposition analysis with Hyperion data. Journal of Applied Remote Sensing, 4(1), 043520.

60. Assaf, A.; Compton, J.T. Historical Perspectives on AVHRR NDVI and Vegetation Drought Monitoring. 2011. Available online: https://ntrs.nasa.gov/api/citations/20110014328/downloads/20110014328.pdf (accessed on 13 April 2025).

61. Otgonbayar, M.; Atzberger, C.; Chambers, J.; Damdinsuren, A. Mapping pasture biomass in Mongolia using Partial Least Squares, Random Forest regression and Landsat 8 imagery. Int. J. Remote Sens. 2018, 40, 3204–3226. [CrossRef]

62. Available online: https://www.eoportal.org/satellite-missions/prisma-hyperspectral (accessed on 7 January 2025)

List of Publications

SELECTED PUBLICATIONS:

1. Margad-Erdene Jargalsaikhan*, Dorj Ichikawa, Masahiko Nagai, Tuvshintogtokh Indree, Vaibhav Katiyar, Davaagerel Munkhtur, Erdenebaatar Dashdondog, "*Aboveground Biomass Estimation and Time Series Analyses in Mongolian Grasslands Utilizing PlanetScope Imagery*", Remote Sensing. 2024, *16*(5), 869. [CrossRef]
2. Margad-Erdene Jargalsaikhan*, Masahiko Nagai, Begzsuren Tumendemberel, Erdenebaatar Dashdondog, Vaibhav Katiyar, and Dorj Ichikawa, "*Adapting the High-Resolution PlanetScope Biomass Model to Low-Resolution VIIRS Imagery Using Spectral Harmonization: A Case of Grassland Monitoring in Mongolia*", Remote Sensing. 2025, 17(8), 1428. [CrossRef]

CONFERENCE PAPER AND PRESENTATIONS:

3. Margad-Erdene Jargalsaikhan*, Dorj Ichikawa, Masahiko Nagai, Tuvshintogtokh Indree and Vaibhav Katiyar, "*Analyzing Grazing-Induced Changes in Mongolian Grasslands using PlanetScope Imagery*", IGARSS 2024 - 2024 IEEE International Geoscience and Remote Sensing Symposium, Athens, Greece, 2024, pp. 2700-2704; oral presentation. [CrossRef]
4. Jargalsaikhan Margad-Erdene, Dorj Ichikawa, Vaibhav Katiyar, Masahiko Nagai, "*Multi-temporal monitoring for the grazed and ungrazed vegetation dynamics of Mongolian grassland using PlanetScope imagery*" 34th International Symposium on Space Technology and Science; Kurume in Fukuoka, Japan, 2023, oral presentation. [CrossRef]
5. Margad-Erdene Jargalsaikhan*, Dorj Ichikawa, Masahiko Nagai, Tuvshintogtokh Indree, Davaagerel Munkhtur, "*High-Resolution PlanetScope Imagery Utilization for Biomass Estimation and Time Series Mapping in Mongolian Grasslands*", International Conference on Plant Science; Ulaanbaatar, Mongolia, 2024, oral presentation.
6. Margad-Erdene Jargalsaikhan, Masahiko Nagai, Dorj Ichikawa, "*Application of VIIRS Imagery for Large-Scale Grassland Monitoring*", 8th Human Resource Development and Space Data Utilization for Disaster Symposium; Indonesia, Bali, 2025, oral presentation.
7. Jargalsaikhan Margad-Erdene, Masahiko Nagai, Dorj Ichikawa "*Spectral Harmonization of High-Resolution PlanetScope to Low-Resolution JPSS-VIIRS Imagery for Grassland*

Monitoring" International Symposium on Remote Sensing 2025 (ISRS 2025); Incheon, Korea, 2025, oral presentation. [CrossRef]

8. Jargalsaikhan Margad-Erdene, Dorj Ichikawa, Masahiko Nagai "Optimized Spectral *Harmonization for Biomass Model Adaptation in Grassland Monitoring*" The 19th International Conference on Algorithmic Aspects in Information and Management (AAIM 2025); Ulaanbaatar, Mongolia, 2025, oral presentation. [CrossRef]